DEVELOPMENT OF DATA UNFOLDING
TECHNIQUES FOR CONTOURED SEMICONDUCTOR
NEUTRON SPECTROMETER

by

James A. Shannon

prepared for

NATIONAL AERONAUTICS AND SPACE ADMINISTRATION

contract   NAS 8-11631

SPACE SCIENCES LABORATORY
GENERAL ELECTRIC
MISSILE AND SPACE DIVISION

Requests for copies of this report should be referred to

National Aeronautics and Space Administration
Office of Scientific and Technical Information
Attention: AFSS-A
Washington, D.C. 20546

FINAL REPORT

DEVELOPMENT OF DATA UNFOLDING TECHNIQUES FOR CONTOURED SEMICONDUCTOR NEUTRON SPECTROMETER

by

James A. Shannon

prepared for

NATIONAL AERONAUTICS AND SPACE ADMINISTRATION

July 1, 1965

CONTRACT NAS 8-11631

TABLE OF CONTENTS

I. INTRODUCTION

This report covers the work performed in the period 29 June 1964 through 29 June 1965, concerning the investigation of a technique for measuring neutron spectra. Briefly, one is required to deduce the neutron spectrum incident on a crystal of silicon from a knowledge of the energy of the charged particles resulting from the reactions Si (n, α) and Si (n, p). Thus, the essential part of such a spectrometer would consist of a silicon crystal with a sensitive region which is placed in a neutron environment, and a charged particle energy analyzer to record the charged particle spectrum. Such a technique is particularly inviting because alternative methods of measuring neutron spectra involve a considerably more complex procedure than that envisioned here.

For this approach to be fruitful, one requires (1) knowledge of the physics of the neutron-silicon interaction throughout the energy range of interest, (2) a silicon detector capable of living in a neutron environment for a length of time sufficient to record useful charged particle spectra and (3) a system for measuring the energy of the resultant α-particles and protons.

We have made some progress concerning the physics of the neutron-silicon and its application to neutron spectroscopy. These subjects form the bulk of this report.

Concerning a suitable silicon detector, we have fabricated two detectors of diameter 0.8 cm and depletion depth $\sim$ 500 microns. These are similar to those provided the NASA under Contract NAS 8-5395 and they appear to be an order of magnitude more resistant to neutron damage than other types of detectors. A brief discussion of these detectors is contained in Chapter III.

Measuring equipment used in this study consisted of a commercial charge amplifier, pulse height analyzer, power supplies, and printer. These are laboratory devices and are not really suited to a space environment. However, we understand similar equipment suitably engineered for a space environment is available from several reputable firms. Some

details of the telemetry system for transmitting the required data by an r.f. link have been worked out and are included in Chapter IV.

The following conclusions are discussed in Chapter V of this report.

1. A portion of the energy spectrum of a neutron source with no neutrons of energy greater than 10.4 MeV may be measured with this technique. This portion is limited to the energy range greater than 5.2 MeV. The technique works best with sources when the time scale is less than 2 minutes.

2. In general, the poorer the resolution, the more suitable is this technique. Thus, one must use the poorest resolution consistent with the spectral knowledge required. 400 keV is suggested as being adequate and 200 keV should be attainable.

3. A similar technique using crystals constructed from the comparatively rare isotope, Si-29, gives one the possibility of measuring neutron spectra down to the keV region. Gram quantities of Si-29 must be available before such a crystal can be constructed.

4. The signals required for operation of this technique are well within the capability of present telemetry technology.

A preliminary discussion of the technique discussed in this report was presented at the 11th Nuclear Science Symposium on October 28 last[1]. A paper discussing the Si (n, q) interaction at 9-10 MeV, based on some of the work discussed in Chapter III will be submitted to the Physical Review. A paper on the overall method is being prepared for submission to Nuclear Instruments and Methods.

REFERENCE

1. J. A. Shannon, J. B. Trice and G. C. Huth, IEEE Transactions on Nuclear Science, NS-12, 281 (1965).

II. METHOD OF SOLUTION

A. OUTLINE OF SOLUTION

Let $\Phi(E_n)$ be the, in general unknown, spectrum of neutron flux incident on a silicon crystal. If $\sigma_1(E_q, E_n)$ is the cross section for a neutron of energy, E_n, to induce the Si (n, q) reaction, where the energy of the charged particle, q, is between E_q and $E_q + d E_q$, then the crystal will be expected to have a charged particle spectrum $d N (E_q)/d E_q$, such that

$$\frac{d N (E_q)}{d E_q} = \int_0^\infty \Phi(E_n) \cdot d E_n \cdot \sigma_1(E_q, E_n) \cdot N_1 \qquad (2.1)$$

$$\frac{Number}{MeV} = \frac{Number}{MeV} \cdot MeV \cdot \frac{Millibarn}{MeV} \cdot \frac{Number\ of\ Si\ nuclei}{Millibarn}$$

The units in which each term is measured are indicated.

Equation 2.1 is to be solved for $\Phi(E_n)$ when $d N (E_q)/ d E_q$, $\sigma_1(E_q, E_n)$ and N_1 are known. This is an integral equation of the first kind with the kernel, $\sigma_1(E_q, E_n)$, being a non-symmetric function of its arguments. There are no analytic procedures for finding a solution to such an equation, but, since the equation is applicable to a wide range of problems, it has been attacked many times.

For example, much of our knowledge of the photonuclear effect comes from yield measurements of nuclei which are irradiated by electron brems-strahlung. In this instance, the activation yield corresponds to $d N (E_q)/d E_q$ in equation 2.1; the bremsstrahlung spectrum corresponds to $\sigma_1(E_q, E_n) \cdot N_1$, and the unknown, $\Phi(E_n)$ is the photonuclear cross section which one seeks to find.

In the photonuclear context, the equation has been successfully solved by approaches differing among themselves only in detail.[1-3] The approach used here most closely resembles that of Penfold and Leiss[2].

One approximates Equation 2.1 by taking finite and equal energy intervals, ΔE_q and ΔE_n, along the charged particle energy axis and the neutron energy axis,

$$\Delta N (E_{q,j}) = \sum_{i=1}^{\infty} \Phi(E_{n,i}) \Delta E_n \overline{\sigma_1 (E_{q,j}, E_{n,i})} N_1 \cdot \Delta E_q . \qquad (2.2)$$

3

where $\overline{\sigma_1(E_{q,j}, E_{n,i})}$ is some average value of $\sigma_1(E_q, E_n)$ in the energy square $E_{q,j} < E_q < E_{q,j+1}$; $E_{n,i} < E_n < E_{n,i+1}$. Since real neutron spectra do not extend to infinite energies, the upper limit, ∞, in the integration and summation may be replaced by a finite value.

For a fixed value of neutron energies, E_n, the charged particle spectrum, which is proportional to σ_1, consists of a series of peaks, each peak corresponding to a reaction where the residual nucleus is left in a definite state. See Figure 2.1. This state is, in general, an excited one. Its subsequent de-excitation can be troublesome but let us ignore this point now.

Each excited state has a finite width associated with it. Since these widths are not generally known and since they must be small compared with the distance between states, it is reasonable to approximate σ_1 by a δ function

$$\sigma_1(E_q, E_n) \cong \sigma(E_q, E_n) \delta(E_q - E_n - Q). \tag{2.3}$$

σ, as given by equation 2.3 is the quantity to be used in the subsequent analysis. It has a different meaning from σ_1 and is measured in different units (millibarn). Q is the energy difference between the states (neutron at rest + Si nucleus in ground state) and (residual excited nucleus + residual charged particle at rest). Q is negative for the interactions of neutrons with silicon. In Appendix A are tables of the various residual states to be expected in the Si (n, q) interactions. Appendix B tabulates the Q values of the reaction and the various spins of the residual nucleus.

Substituting 2.3 into 2.2 and integrating out the δ function, one finds

$$N(E_{q,j}) = \sum_{i=1}^{M} \Phi(E_{n,i}) \cdot \Delta E_n \cdot \overline{\sigma(E_q, E_n)} \cdot N_1 \tag{2.4}$$

In 2.4, one has, instead of the integral equation 2.1, a set of M simultaneous linear equations to be solved for the values of neutron spectra, $\Phi(E_{n,i})$. The matrix corresponding to $\Delta E_n \cdot \overline{\sigma(E_q, E_n)}$ is to be solved once for all by inversion so that

$$\Phi(E_{n,j}) = \frac{1}{N_1 \cdot \Delta E_n} \cdot \sum_{i=1}^{M} \overline{\sigma(E_q, E_n)}^{-1} \cdot N(E_{q,i}). \tag{2.5}$$

4
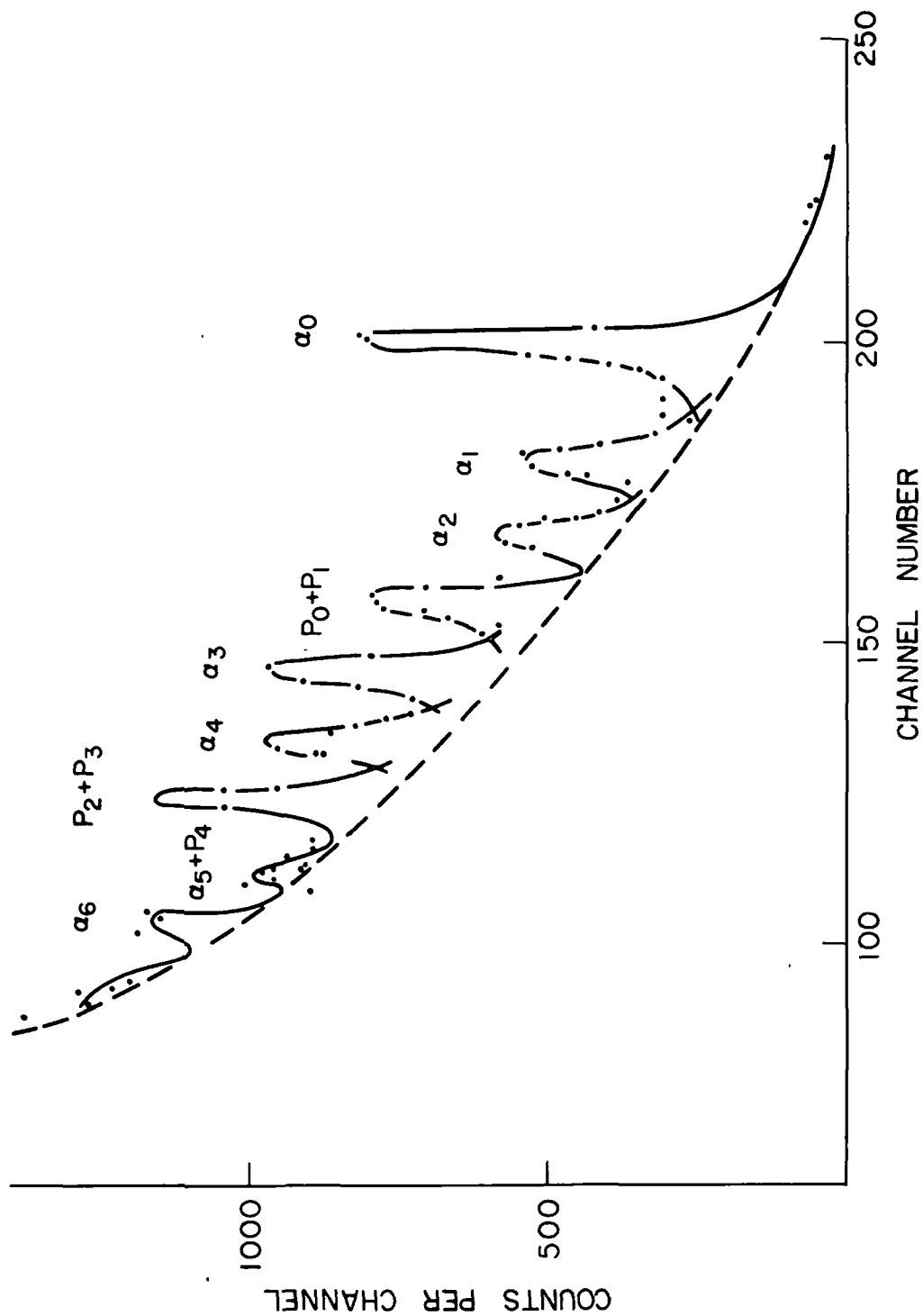
Figure 2.1. The Si (n, q) reaction at 9.5 MeV neutron energy. The peaks corresponding to α_0, α_1, α_2, $p_0 + p_1$, etc., sit on top of a continuous charged particle distribution. The peak at α_0 corresponds to the Si^{28} (n, α) Mg^{25} reaction when the Mg nucleus is left in the ground state. Similarly the $p_0 + p_1$ peak corresponds to the reaction Si^{28} (n, p) Al^{28} where the residual nucleus is left in its ground state, or very near it. (.031 MeV).

5

If all values on the right hand side of 2.5 are known, the problem may be considered to be solved in principle.

As will be seen below, the quantity σ (E_q, E_n) is reasonably well known up to E_n = 10.4 MeV neutron energy. For a polyergic neutron flux with no neutrons of energy greater than 10.4 MeV, there is experimental authority to construct the cross section σ (E_q, E_n) and hence, the matrix elements to be inserted in Equations 2.4 and 2.5. This energy limit does not seriously inhibit the application of the method, however. The prompt neutron flux from thermal fission has negligible flux of neutrons with energy greater than 10.4 MeV.

B. EVALUATION OF THE QUANTITY σ (E_q, E_n)

Because the Si (n, p) Al or Si (n, α) Mg interactions leave the residual Al or Mg nucleus in a definite excited state, the cross section σ (E_q, E_n) to be used in Equation 2.4 has a very simple representation in E_q, E_n, σ space. It is a set of plane curves, the planes being perpendicular to the E_q - E_n plane, all planes parallel and lying along the lines E_q - E_n = Q as in Figure 2.2. The value of σ is zero except along the diagonal lines where it has values given by the numbers near the lines. The level represented by each line is defined at the upper end of that line.

To take an example, the cross section for neutrons of energy 8.5 MeV to undergo a Si (n, q) reaction yielding a charged particle of energy 4.66 MeV has a value of 110 mb. The label on the upper end of the line shows that the reaction is Si^{28} (n, p_0 + p_1) Al^{28} and that the residual nucleus is left either in its ground state, p_0, or its first excited state, p_1, these states being indistinguishable experimentally. The Si^{28} (n, q) interaction at 8.5 MeV neutron energy also leads to charged particles with the values of charged particle energy and cross sections shown in Table 2.1.

Besides Si^{28}, natural silicon contains isotopic impurities of Si^{29} (4.7%) and Si^{30} (3%). Furthermore, the Si^{29} (n, q) and Si^{30} (n, q) cross sections must be expected to be of the same order of magnitude as the cross sections shown in Figure 2.2. However, the small quantities of these isotopes in a
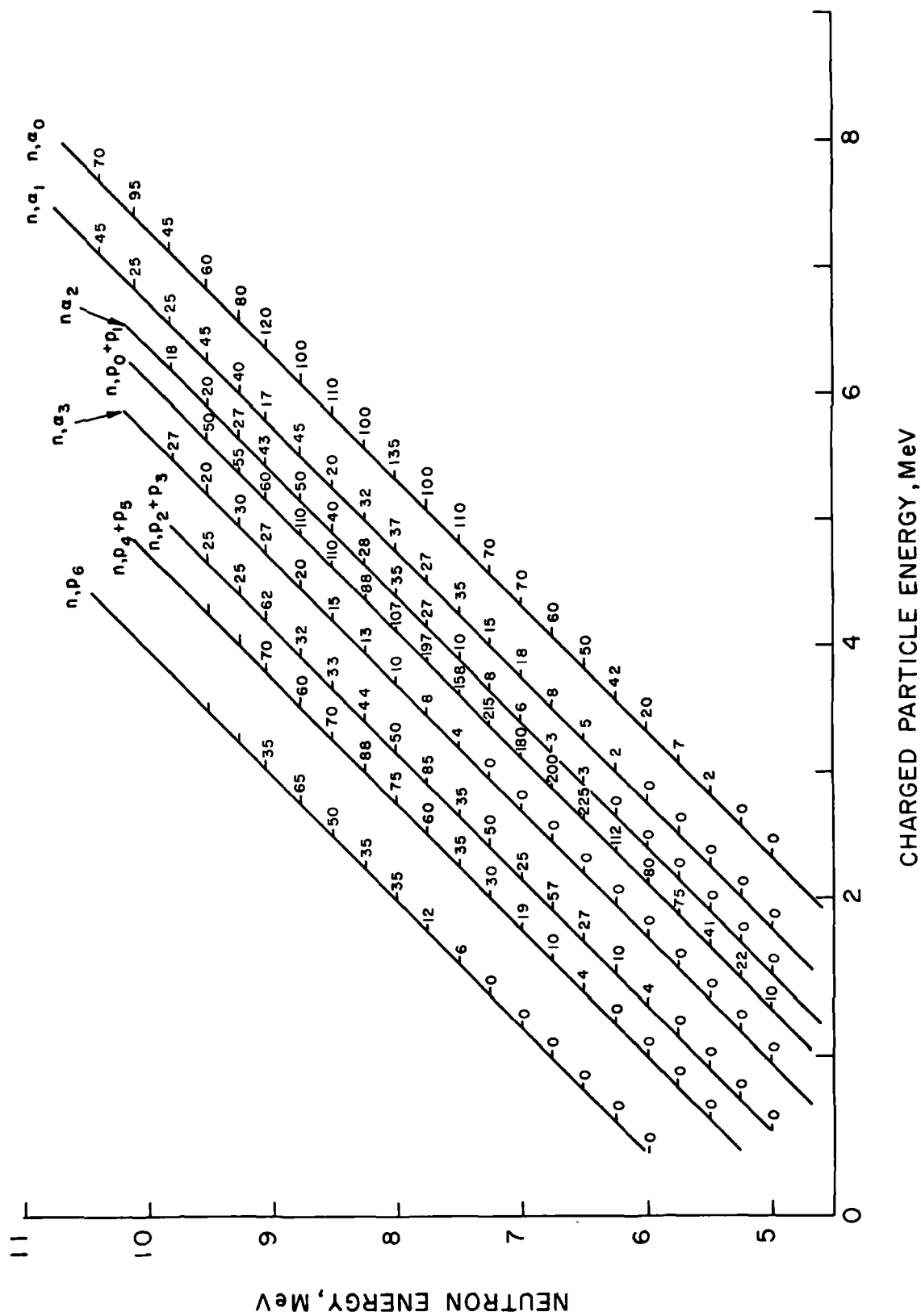
Figure 2.2. Values of the Cross Section σ(E_q, E_n). σ is zero everywhere except along the diagonal lines where it has the value in mb given by the number near the lines. Characteristics of the residual nucleus are shown by labels at the top of the lines.

7

TABLE 2.1

Values of charged particle energy associated with the 8.5 MeV neutron interaction on silicon.

Charged Particle Energy	Cross Section
2. 50 MeV	50 mb
3. 25	70
3. 62	33
4. 23	15
4. 66	110
4. 90	40
5. 27	20
6. 10	110

detector made of natural silicon imply that the Si[29] and Si[30] interactions can be ignored in the neutron energy region when the Si[28] (n, q) reaction is energetically possible.

The values of the most of the cross sections shown in Figure 2.2 have been taken from the work of Andersson-Lindström.[4] He and a group at Rice[5] determined the various cross sections Si[28] (n, q) with neutrons of energy up to 9.2 MeV. The data of both investigators are similar, as shown in Figures 2.3 and 2.4, although those of the Rice group appears to have values some 20% higher than those of Andersson-Lindström.

Data points for neutron energies above 9.2 MeV were determined during the course of this investigation. See Chapter III.

C. CONSTRUCTION OF THE MATRIX FROM $\overline{\sigma (E_q, E_n)}$

From the graph of Figure 2.2, a matrix may be evaluated with elements given by the formula

$$M_{ij} = \overline{\sigma (E_q, E_n)} \quad . \tag{2.6}$$

Such a formulation may be visualized as follows: Construct a square net of sides $\Delta E_n \times \Delta E_q$ to be dropped in imagination over the graph. This will cut the $E_q - E_n$ plane in a series of squares of area $\Delta E_n \times \Delta E_q$. The value of the matrix element (2.6) is proportional to the mass of that part of the perpendicular plane seen on edge in Figure 2.2 which is contained in the square $(E_{n, i+1} - E_{n, i})$, $(E_{q, j+1} - E_{q, j})$.

One must be very perspicacious in choosing the size of the net if the errors associated with the set of equations, 2.5, is to be minimized. The matrix used in 2.4 must have an inverse if one is to perform the operation indicated by 2.5. This means that the matrix of 2.4 must be a square matrix and, in order that its inverse be "well behaved", it should be diagonally dominant,

$$M_{ii} > M_{ij} \quad j \neq i . \tag{2.7}$$

The condition, 2.7, is made reasonable on the grounds that if we have

$$M_{ii} >> M_{ij} \tag{2.8}$$

Figure 2.3.   Si (n, p) Al Cross Sections.   Values in mb.   From BNL-325[6]
and present work.
  o   Rice Group.   Cf. Reference 5.
  ●   Andersson-Lindström.   Cf.   Reference 4.
  x   Present work.
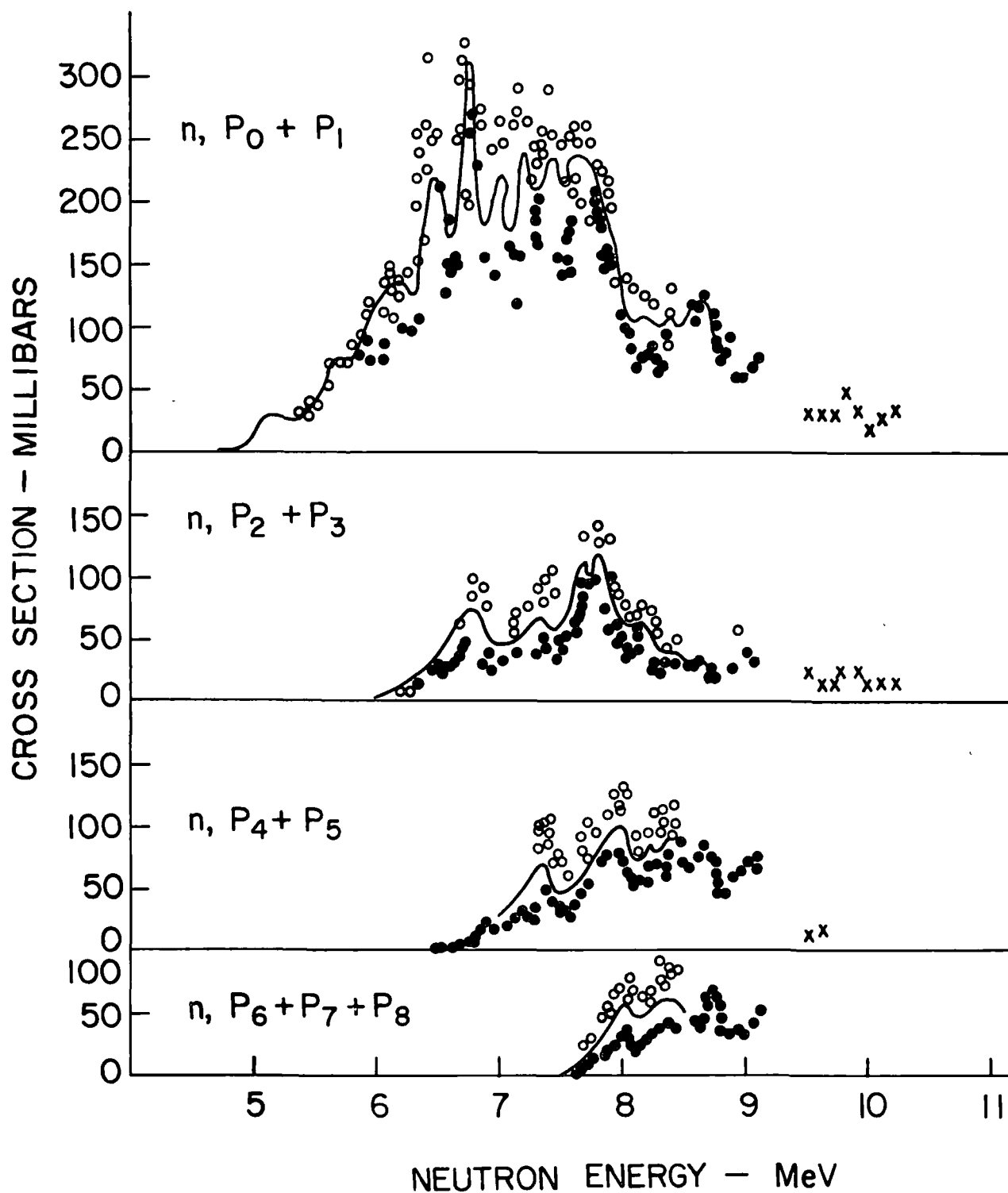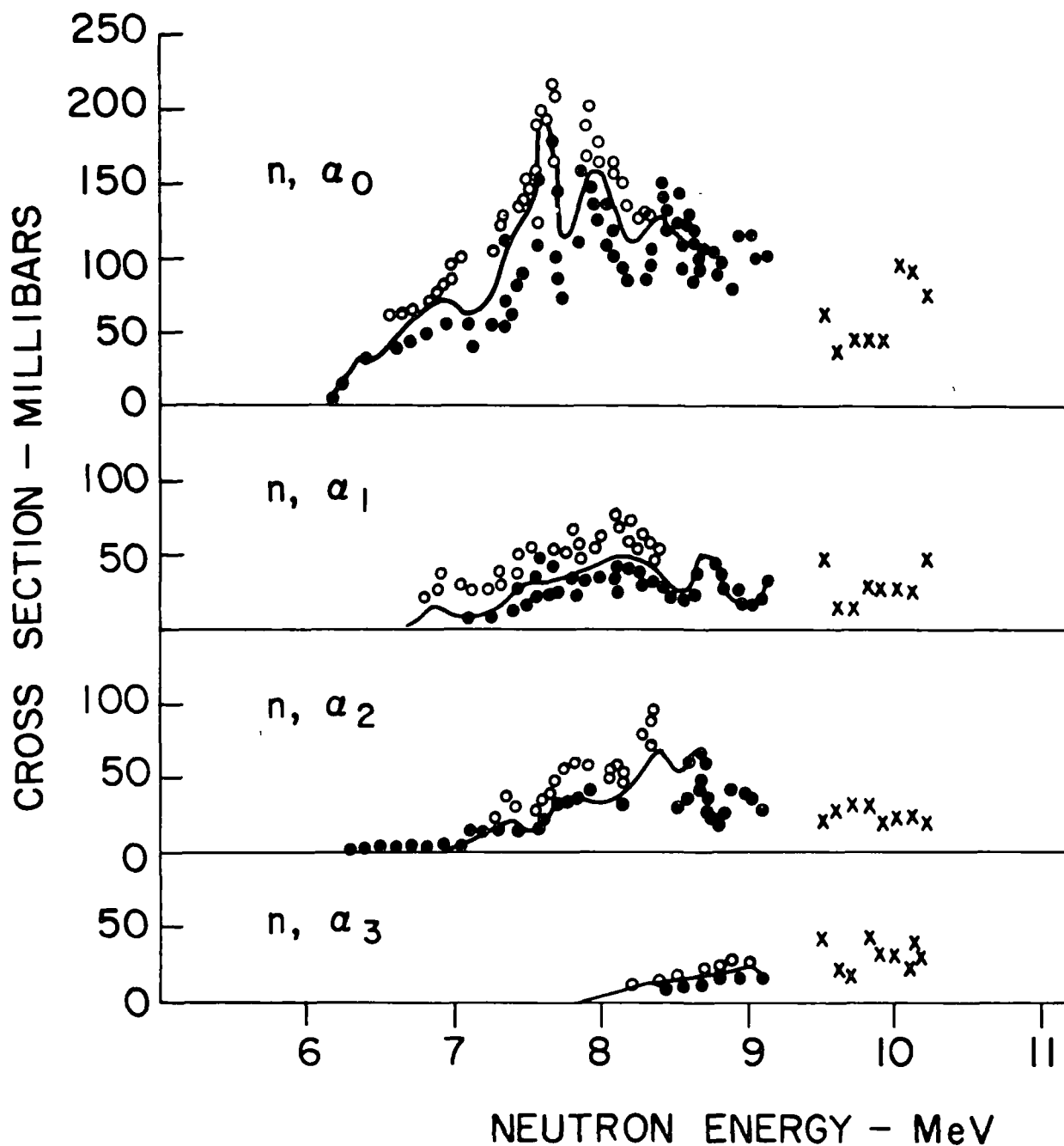
10

Figure 2.4.   Si (n, α) Mg Cross Sections.   Values in mb.   From BNL-325[6]
and present work.
o   Rice Group.   Cf. Reference 5.
●   Andersson-Lindström.   Cf. Reference 4.
x   Present work.

11

then the inverse matrix is also diagonal and there is a one-for-one correspondence between a neutron in bin E_x and a charged particle in its corresponding bin.

Starting with the general rule for inverting a diagonally dominant matrix,

$$\lim_{e,f,g\ldots \to 0}
\begin{bmatrix}
a_1 & e_1 & e_2 \cdots \\
f_1 & a_2 & f_2 \cdots \\
g_1 & g_2 & a_3 \cdots \\
\cdot & \cdot & \cdot \\
\cdot & \cdot & \cdot \\
\cdot & \cdot & \cdot
\end{bmatrix}^{-1}
=
\begin{bmatrix}
a_1^{-1} & \dfrac{-e_1}{a\,a_2} & \dfrac{-e_2}{a_2\,a_3} \cdots \\
\dfrac{-f_1}{a_1\,a_2} & a_2^{-1} & \dfrac{-f_2}{a_2\,a_3} \cdots \\
\dfrac{-g_1}{a_1\,a_3} & \dfrac{-g_2}{a_2\,a_3} & a_3^{-1} \cdots \\
\vdots & \vdots & \vdots
\end{bmatrix}
\qquad (2.9)$$

one may write an analytic expression for the approximation for the neutron flux in any bin, in particular bin E_{n1}.

$$\Phi(E_{n1}) = \frac{1}{\sigma(E_{n1}, E_q = E_{n1} - 3870) \cdot N_1 \cdot \Delta E_n} \cdot \left[N(E_{q1}) - \sum_{i=2}^{K} \frac{\sigma(E_{n1}, E_{qi})N(E_{qi})}{\sigma(E_{ni} = E_{qi} - 3870, E_{qi})} \right]$$

$$(2.10)$$

Equation 2.10 is written in the form shown because one obvious way to construct a matrix net for the graphs of Figure 2.2 is to take the diagonal along the line representing the cross section for Si^{28} (n, $p_0 + p_1$) Al^{28}. The Q-value for this reaction, -3870 keV, enters several times in equation 2.10.

The square of the standard deviation associated with 2.10 is

$$\frac{1}{\left[\sigma(E_{n1}, E_q = E_{n1} - 3870) \cdot N_1 \cdot \Delta E_n \right]^2} \cdot \left[N(E_{q1}) + 2 \sum_{i=2}^{K} \frac{\sigma(E_{n1}, E_{q1})}{\sigma(E_{ni} = E_{qi} - 3870, E_{qi})} \cdot N(E_{qi}) \right]$$

$$(2.11)$$

Although the approximations used in arriving at equation 2.10 and 2.11 make them virtually useless for actual calculations, they may serve as guides to further define the matrix net.

The ratios of off-diagonal to diagonal cross sections appearing in 2.11 are independent of the coarseness of the net. The total number of significant ratios, however, is directly proportional to the number of bins defining the size of the net and hence varies as $(\Delta E_n)^{-1}$. Thus, one must use a net as coarse as is consistent with the spectral information which is required.

A study of Figure 2.2 reveals the following: (1) The lower limit of usefulness of this method is about 5.2 MeV. Below this energy, the relevant cross sections fall rapidly to zero. (2) If one is interested in any portion of the neutron spectrum between 5.2 and 8.5 MeV, then he should diagonalize along the line $(n, p_0 + p_1)$. (3) If the interest is in any portion of the spectrum above 8.5 MeV, then the diagonal should be taken along the line (n, α_0).

Figure 2.5 is the matrix using a net of $\Delta E_n = \Delta E_q = 400$ keV constructed from Si^{28} (n, q) data such as that represented in Figure 2.2. The matrix is non-square and as such may not be used directly in Equation 2.5. However, one may take a square submatrix of Figure 2.5 which can be used in Equation 2.5. The form of this submatrix depends on whether that part of the neutron energy spectrum below or above 8.5 MeV is of interest.

The 13 x 13 square submatrix defined by $5.2 < E_n < 10.4$ MeV, $1.34 < E_q < 6.54$, and shown above the dashed line in Figure 2.5 may be used to define the neutron flux in any bin with $E_n < 7.5$ MeV. For a bin with $E_n > 8.8$ MeV, it would be preferable to work with the 6 x 6 matrix defined by the solid lines. In general, the cross-over point may be taken as 8.5 MeV above which the cross section for Si^{28} (n, α_0) dominates that for Si^{28} $(n, p_0 + p_1)$.

It will be noted that zeroes have been placed in the upper right hand corner of Figure 2.5 despite the fact that these cross sections have not been accurately measured. This should not be too poor on approximation, however,

Neutron Energy From → To		5.2 5.6	5.6 6.0	6.0 6.4	6.4 6.8	6.8 7.2	7.2 7.6	7.6 8.0	8.0 8.4	8.4 8.8	8.8 9.2	9.2 9.6	9.6 10.0	10.0 10.4
Charged Particle Energy From	**To**													
1.343MeV	1.743MeV	37.4	0	6.2	14.0	8.2	3.2	2.9	φ	φ	φ	φ	φ	φ
1.743	2.143	0	86.3	0	19.5	35.1	22.2	14.1	10.0	φ	φ	φ	φ	φ
2.143	2.543	0	0	108.5	0	23.3	43.8	28.1	24.4	17.5	φ	φ	φ	φ
2.543	2.943	0	0	1.6	188.	0	28.4	85.7	26.4	35.3	13.6	φ	φ	φ
2.943	3.343	0	8.0	2.3	3.7	184.6	1.9	45.9	59.2	33.7	32.1	φ	φ	φ
3.343	3.743	0	0	27.2	2.3	12.14	178.	5.6	19.6	53.7	23.8	φ	φ	φ
3.743	4.143	0	0	0	50.	7.0	14.9	191.5	9.3	17.7	52.6	φ	φ	φ
4.143	4.543	0	0	0	0	62.	18.0	32.0	99.8	14.0	25.6	16.0	φ	φ
4.543	4.943	0	0	0	0	0	91.	18.	33.7	131.4	27.9	22.	14.3	φ
4.943	5.343	0	0	0	0	0	0	127.8	17.4	46.6	85.4	67.	20	11.2
5.343	5.743	0	0	0	0	0	0	0	105.	20.3	31.2	72.6	55.	14.7
5.743	6.143	0	0	0	0	0	0	0	0	112.	13.5	50.4	88.7	53.0
6.143	6.543	0	0	0	0	0	0	0	0	0	105.	40.5	33.7	67.6
6.543	6.943	0	0	0	0	0	0	0	0	0	0	112.	27.1	42.0
6.943	7.343	0	0	0	0	0	0	0	0	0	0	0	105.	52.4
7.343	7.743	0	0	0	0	0	0	0	0	0	0	0	0	170.

Figure 2.5. Matrix of $\sigma (E_n, E_p)$

14

as the nuclear coulomb barrier is quite effective in prohibiting the (n, q) reaction when low energy charged particles are involved.

The inverse of the two square submatrices indicated in Figure 2.5 were computed by machine. They are shown as Figures 2.6 and 2.7. The matrix of Figure 2.6 is to be used for calculating flux for the neutron energies $5.2 < E_n < 8.4$ MeV and that of Figure 2.7 for the same calculations when the bins in the energy interval $8.4 < E_n < 10.4$ MeV are required.

D. ERRORS

There will be systematic and statistical errors associated with this method. A study of Figures 2.3 and 2.4 suggests that the relevant cross sections are fairly reproducible among themselves although the absolute values may have an error of about 20%. Andersson-Lindström and Rössle[4] estimate their relative values as accurate to about 6%. Assuming that four terms are involved in going from a matrix such as those in Figure 2.5 to its inverse, systematic errors of the order of 15% may be expected for each value of the inverse matrix. The systematic errors will be proportional to the square root of the number of effective terms needed to take an inverse. As only two or three terms dominate the inverse matrix (See Figures 2.6 and 2.7), the overall systematic error should also be of the order of 20%.

To consider statistical errors, it is convenient to construct matrices from those of Figures 2.6 and 2.7 where each term, M^2, is the square of the corresponding term in Figure 2.6 or 2.7. These may be conveniently called variance matrices as the square of the variance associated with the reconstruction of the neutron flux at energy E_n, is given by

$$\sigma^2 \left(\Phi (E_n) \right) = \sum_{i=1} M^2 (E_n, E_{qi}) N (E_{qi}).$$ (2.12)

σ^2 as defined in Equation 2.12 is not the square of a cross section. Its units are the square of the corresponding units in which one measures neutron flux. Conveniently, they may be taken as MeV^{-2}. Figures 2.8 and 2.9 show the variance matrices constructed from the inverse matrices.

Inspection of these figures shows the reason for splitting the neutron flux analysis at 8.5 MeV. The variance associated with the high energy

15

$$10^4 \times \dfrac{\left(\sigma (E_n, E_q) \right)^{-1}}{}$$

E_q From:	1.34	1.74	2.14	2.54	2.94	3.34	3.74	4.14	4.54	4.94	5.34	5.74	6.14
To:	1.74	2.14	2.54	2.94	3.34	3.74	4.14	4.54	4.94	5.34	5.74	6.14	6.54
E_n From / To													
5.2 / 5.6	267	1	-12	-23	-16	-9	14	16	16	-9	-1	-1	2
5.6 / 6.0	0	117	9	-16	-11	-36	19	-33	45	-25	22	-22	-16
6.0 / 6.4	0	-1	101	-2	14	-35	8	-74	34	-23	38	-31	20
6.4 / 6.8	0	-2	0	58	17	-4	-17	-46	2	-8	23	-16	9
6.8 / 7.2	0	-5	-9	9	54	31	-39	6	-54	40	-28	24	-20
7.2 / 7.6	0	2	-22	4	-17	91	-19	42	-63	31	-26	27	-21
7.6 / 8.0	0	4	-6	-4	-39	26	15	109	-71	55	-72	59	-40
8.0 / 8.4	0	3	8	-7	-35	-30	28	103	32	-56	19	-9	12
8.4 / 8.8	0	1	13	5	-6	-52	-15	25	91	2	-43	12	0
8.8 / 9.2	0	-12	22	-44	132	-98	164	-392	245	-199	264	-212	142
9.2 / 9.6	0	9	-28	74	-95	116	-282	298	-249	367	-220	141	-124
9.6 / 10.0	0	-17	10	-8	185	-50	293	-568	182	-334	435	-137	68
10.0 / 10.4	0	22	-23	63	-239	108	-231	714	-323	255	-495	313	-33

Figure 2.6. 10^4 Time the Inverse of the 13 x 13 Matrix Indicated in Figure 2.5.

16

Charged Particle Energy, MeV						
From	5.343	5.743	6.143	6.543	6.943	7.343
To	5.743	6.143	6.543	6.943	7.343	7.743

Neutron Energy

From	To						
8.0 MeV	8.4 MeV	95.2	-17.3	-26.1	-44.5	-15.4	23.3
8.4	8.8	0	89.3	-11.5	-36.0	-62.4	4.9
8.8	9.2	0	0	95.2	-34.4	-21.7	-22.7
9.2	9.6	0	0	0	89.3	-23.0	-15.0
9.6	10.0	0	0	0	0	95.2	-29.4
10.0	10.4	0	0	0	0	0	58.8

Figure 2.7. 10^4 Times the Inverse of the 6 x 6 Submatrix Indicated in Figure 2.5.

| | Eq From | 1.34 | 1.74 | 2.14 | 2.54 | 2.94 | 3.34 | 3.74 | 4.14 | 4.54 | 4.94 | 5.34 | 5.74 | 6.14 |
En From	En To \ Eq To	1.74	2.14	2.54	2.94	3.34	3.74	4.14	4.54	4.94	5.34	5.74	6.14	6.54
5.2	5.6	71289	1	144	529	259	81	196	256	256	81	1	1	4
5.6	6.0	0	13689	81	256	121	1296	381	1089	2025	625	484	484	256
6.0	6.4	0	1	10201	4	196	1225	70	5476	1296	529	1444	961	400
6.4	6.8	0	4	0	3136	289	16	289	2116	4	64	529	256	81
6.8	7.2	0	25	81	81	2916	961	1444	36	2916	1600	784	576	400
7.2	7.6	0	4	484	16	289	8281	361	1764	3696	961	676	729	441
7.6	8.0	0	16	24	16	1444	676	225	11881	5041	3025	5184	3481	1600
8.0	8.4	0	9	64	49	1225	900	784	10609	1024	3136	381	81	144
8.4	8.8	0	1	169	25	36	2705	225	625	8281	4	1849	144	0
8.8	9.2	0	144	484	1936	17424	9604	26569	36064	60025	39601	69696	44944	20164
9.2	9.6	0	81	784	5476	9025	13456	79524	88804	62001	134689	48400	19600	15376
9.6	10.0	0	289	100	64	34225	2500	85849	322600	65025	112000	189000	18800	4624
10.0	10.4	0	484	529	3969	57121	11664	53360	509800	104000	65000	245000	98000	1090

10^8 Times Variance Matrix Associated With $\left(\sigma(E_n,\ E_q)\right)^{-1}$

Figure 2.8. Each Element of this Matrix is the Square of the Corresponding Element of Figure 2.6.

		Charged Particle Energy, MeV					
	From	5. 343	5. 743	6. 143	6. 543	6. 943	7. 343
	To	5. 743	6. 143	6. 543	6. 943	7. 343	7. 743

Neutron Energy

From	To						
8. 0 MeV	8. 4 MeV	9063	299	681	1980	237	543
8. 4	8. 8	0	7974	132	1296	3894	24
8. 8	9. 2	0	0	9063	1183	441	515
9. 2	9. 6	0	0	0	7974	529	225
9. 6	10. 0	0	0	0	0	9063	864
10. 0	10. 4	0	0	0	0	0	3457

Figure 2.9. 10^8 times the variance matrix associated with $\left(\sigma(E_n, E_q)\right)^{-1}$. Each element of this matrix is the square of the corresponding element in Figure 2.7.

inverse matrix (Figure 2.9) is far less than that associated with the lower energy matrix (Figure 2.8) for neutron energies above 8.5 MeV.

E. TWO EXAMPLES

We next give examples of the application of these ideas for two cases where they would seem applicable. The first is a thought experiment where the fast neutron spectrum near the fuel rod of a nuclear reactor is analyzed. Then we turn to the results of a real experiment, the measurement of the neutron spectrum from a Pu-α-Be source.

1. Fuel Rod

The energy spectrum of fast neutrons near a fuel rod in a nuclear reactor is expected to be of the form[7]

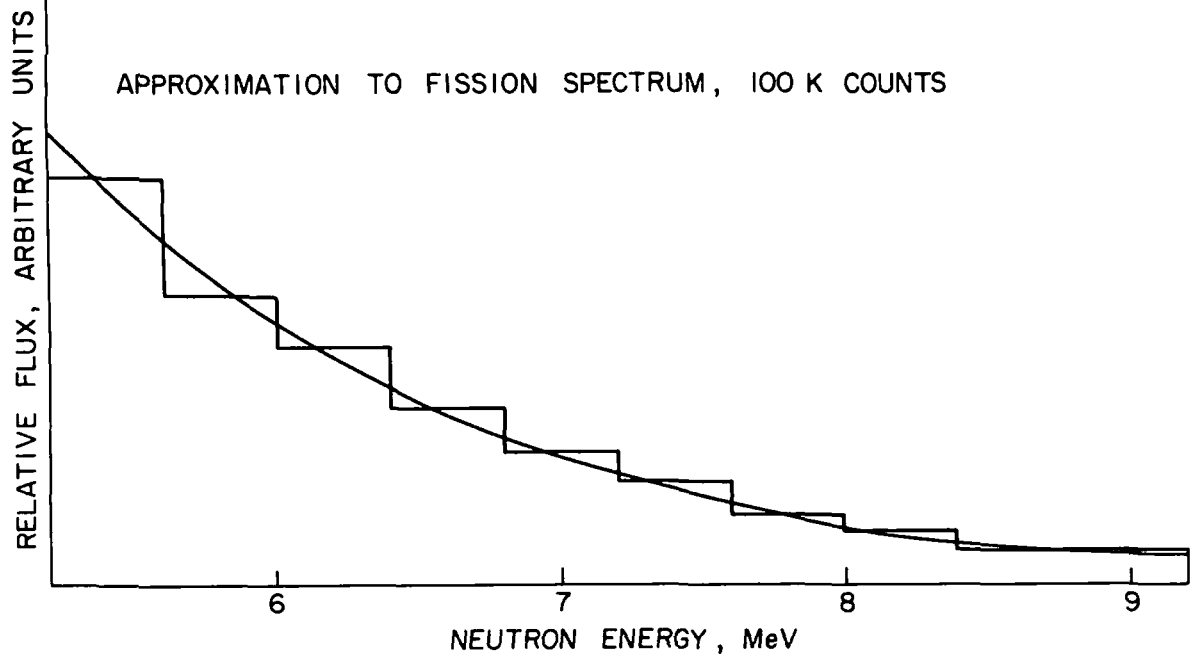$$N(E) \propto \sinh (2E)^{1/2} \cdot e^{-E} \qquad (E \text{ in MeV}), \qquad (2.13)$$

for $E > 1$ MeV. Let us further take the neutron flux as negligible for energies greater than 10.4 MeV, an assumption which may not be too far from the facts.[8] Under the circumstances, the spectrum of Equation 2.13 is particularly suited to our analysis. The relative standard deviation for 100,000 total counts is less than 9% and this only at the highest applicable bin (8.4 - 8.8 MeV). Figure 2.10 a-c summarizes the results of the calculations, taking the computed deviations from the random number table.[9] It appears that even for comparitively few counts, about 1000, that the reconstruction of the spectrum is near perfect.

2. Pu-Be Source

As one may expect, a real experiment is more difficult than a thought experiment. A convenient laboratory source of polyergic neutrons is the Pu-Be$_{13}$ compound which has certain advantages over the more common Po-Be source. The neutron spectrum from Pu-Be has been measured by Stewart[10] using photographic emulsions. Hess has calculated the spectrum to be expected from such a source, assuming that the residual C^{12} nucleus is left in its ground state.[11]

Through the courtesy of L. D. Cohen, the 5 curie Pu-Be source of the Drexel Institute of Technology was made available to us. A brief exposure was taken on 21 April. Details of the experimental procedure are similar to

DEV. 5242

APPROXIMATION TO FISSION SPECTRUM, 100 K COUNTS

RELATIVE FLUX, ARBITRARY UNITS

NEUTRON ENERGY, MeV

DEV. 5239

APPROXIMATION OF FISSION SPECTRUM, 100 K TOTAL COUNTS

RELATIVE FLUX, ARBITRARY UNITS
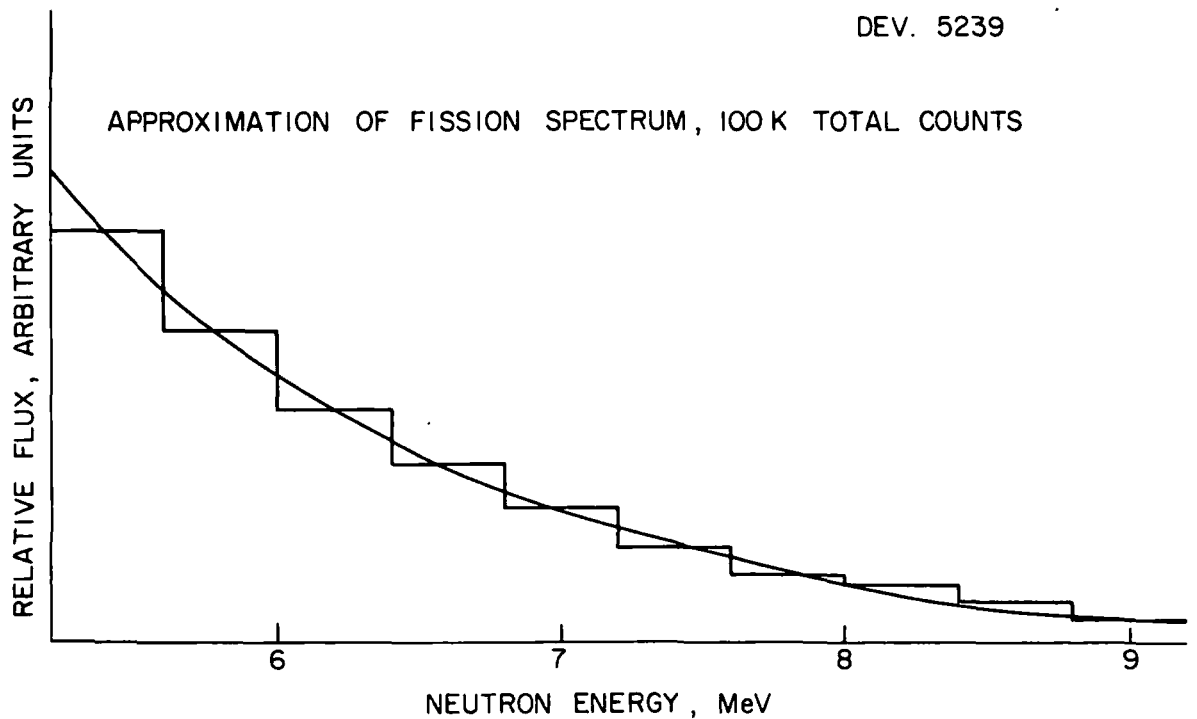
NEUTRON ENERGY, MeV

Figure 2.10 (a). Two reproductions of an assumed neutron spectrum such as that due to nuclear fission. The assumed spectrum is represented by the solid line. Reproduction of this spectrum is shown by the histograms. 100 K total counts.
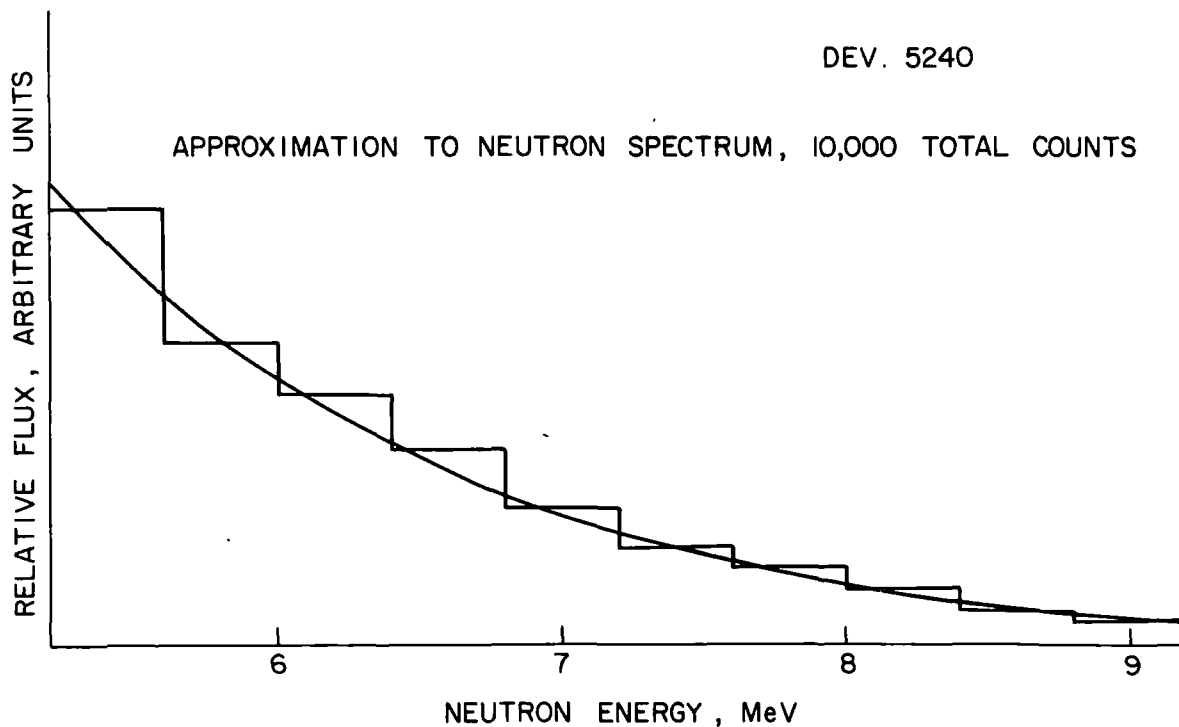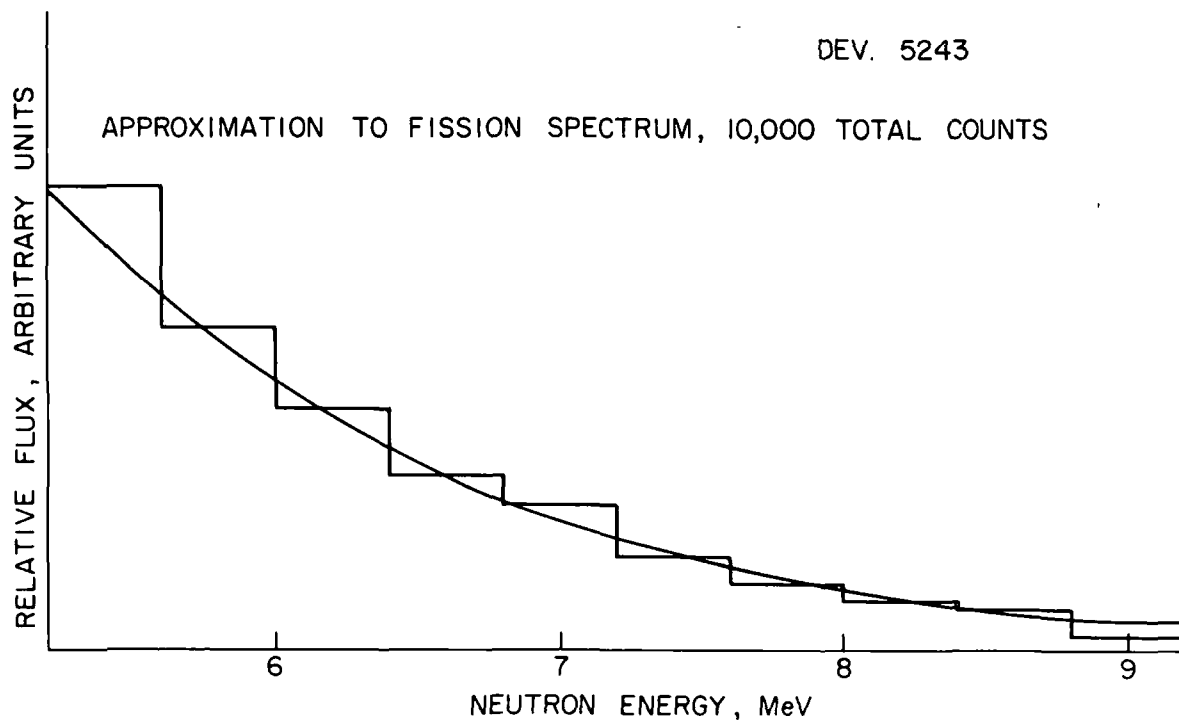
Figure 2.10 (b). Two reproductions of an assumed neutron spectrum such as that due to nuclear fission. The assumed spectrum is represented by the solid line. Reproduction of this spectrum is shown by the histograms. 10 k total counts.

DEV. 5241

APPROXIMATION TO FISSION SPECTRUM, 1,000 TOTAL COUNTS

DEV. 5244

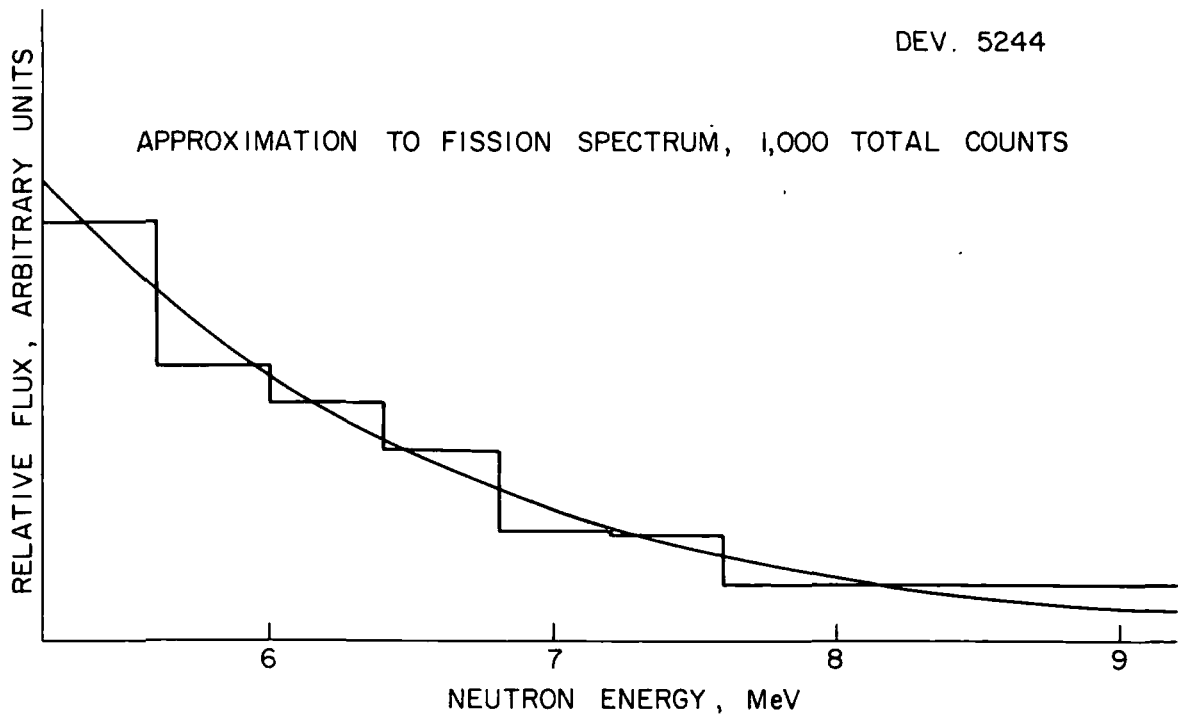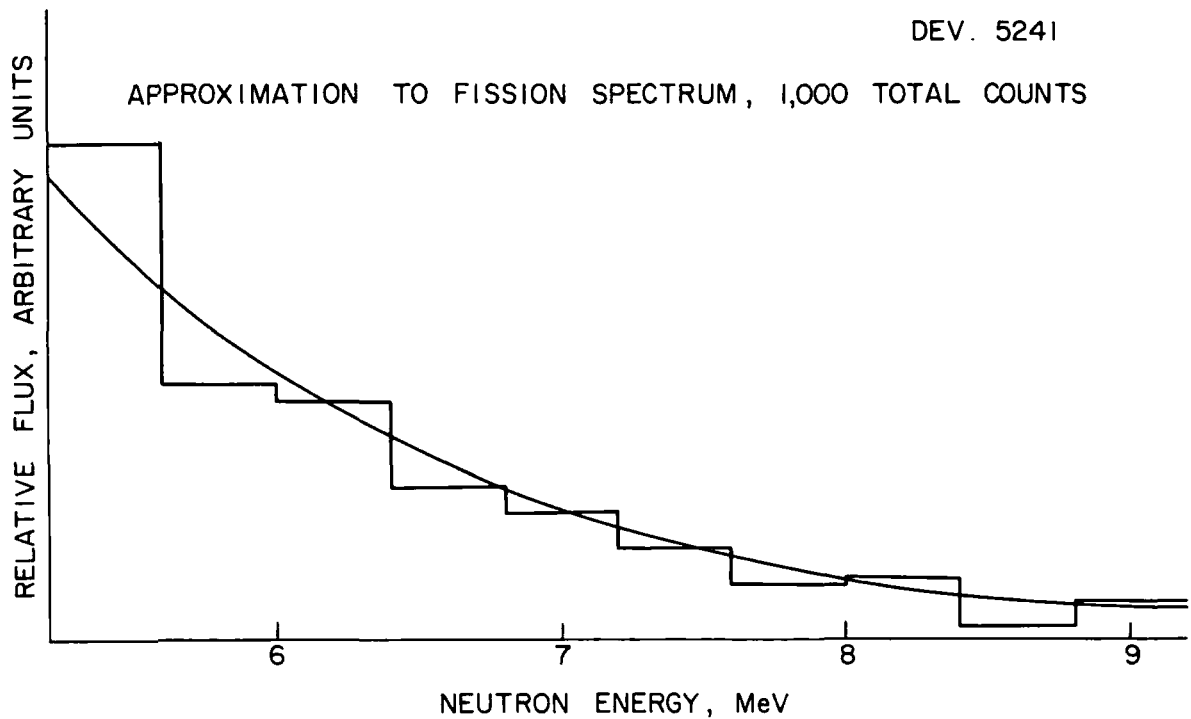APPROXIMATION TO FISSION SPECTRUM, 1,000 TOTAL COUNTS

Figure 2.10 (c). Two reproductions of an assumed neutron spectrum such as that due to nuclear fission. The assumed spectrum is represented by the solid line. Reproduction of this spectrum is shown by the histograms. 1000 total counts.

those used in determining the cross sections $\sigma(E_n, E_q)$ for monoenergetic neutrons and are discussed in connection with that work in Chapter III. There is one important exception, however. When the response to mono-energetic neutrons is to be measured, the charged particle response, $N(E_q)$ is self-calibrating but external calibration is required for a polyergic source.

Calibration of the charge-sensitive amplifier of the system was performed on the 16 April by calibrating a pulse generator against the 5.476 MeV α particles from an Am^{241} source incident on a surface barrier type of solid state detector. Both source and detector are virtually windowless and no correction for windows was made. The location of the charged particle bin boundaries at 1.34, 1.74, 2.14 MeV, etc., were in turn impressed on the pulse height analyzer of the system by adjusting the 10-turn helipot of the pulse generator. One infers from the specifications accompanying the charge sensitive amplifier that this procedure is accurate to within 1.5%. The silicon detector is suitably biased and placed as close to the Pu-α-Be source as possible.

The charge particle spectrum, $N(E_q)$, was displayed on a pulse height analyzer and recorded automatically with suitable equipment. The result of a 90-minute exposure is shown in Figure 2.11.

As the Si^{28} (n, q) cross section falls off rapidly for neutron energies below 5 MeV, the charged particle flux on the left-hand end of Figure 2.11 cannot be expected to be due to the Si (n, q) reaction. that is, one must seek elsewhere besides the (n, q) reaction for the source of charged particle flux with energies below 1.3 MeV. With Mainsbridge, et al[5], we attribute it to the β and γ activity of the residual Al^{28} nucleus. Al^{28} decays with a 2.3 min half life by β - decay, E max = 3.01 MeV, to an excited 1.8 MeV state of Si^{28}. According to Mitchell[12], the Si^{28*} nucleus de-excites by a single γ radiation.

Subtraction of the low energy charged particle spectrum was carried out by adjusting that portion of the spectrum below 1.1 MeV to an exponential function, extending this function past 1.3 MeV and assuming these counts to be due to
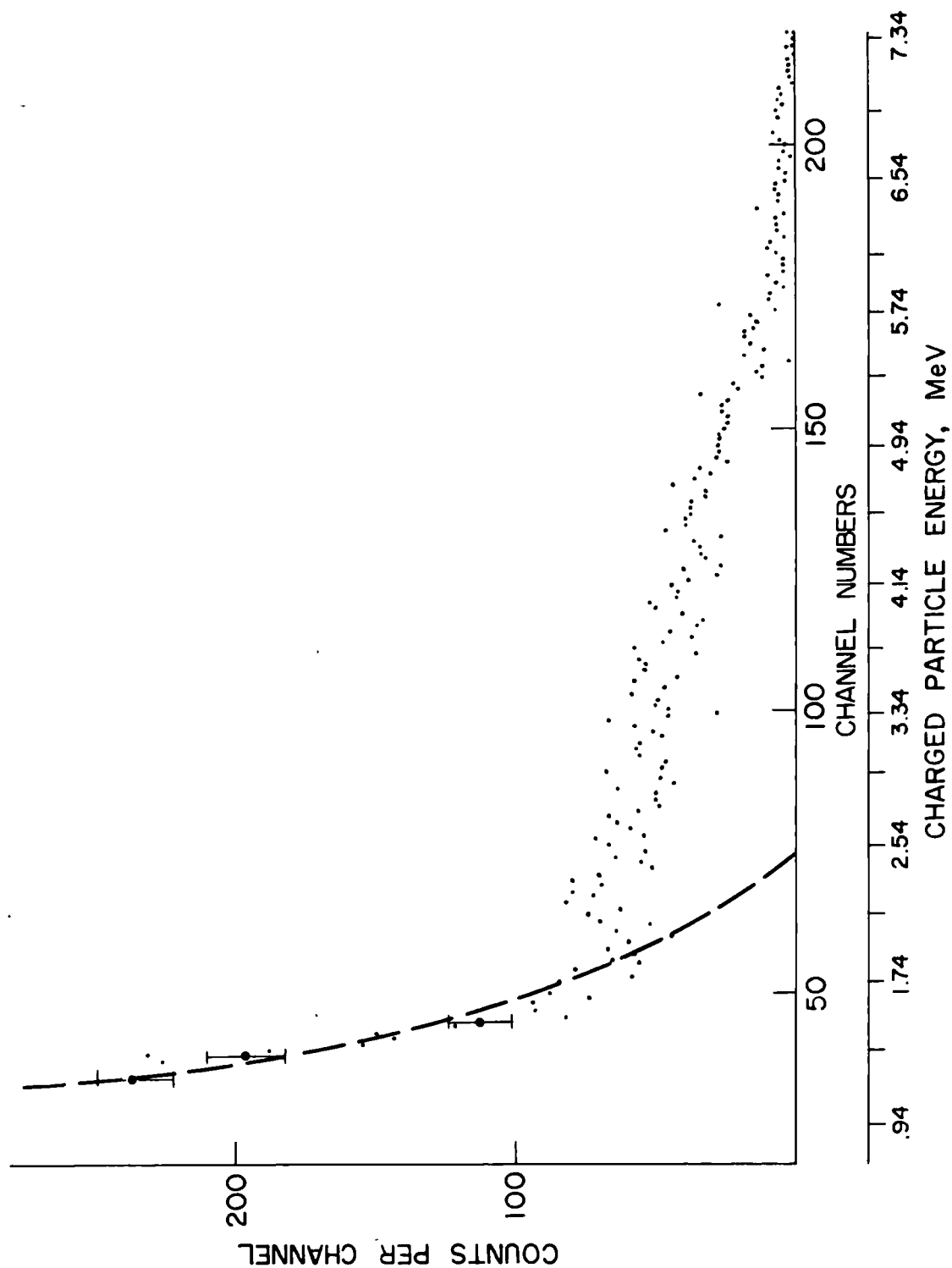
24

Figure 2.11. Charged Particle Response, $N(E_q)$, due to Pu-Be neutrons. Much of the spectrum below 2.9 MeV may be due to the β^- decay of Al^{28}.

the β and γ background. The subtraction was of significance, $> 5\%$, only for the charged particle bins 1.34 - 1.74 and 1.74 - 2.14 MeV.

The result of computing the neutron spectrum with the adjusted matrix is shown in Figure 2.12. For comparison, the measurements of Stewart[10] and the calculations of Hess[11] are also shown.

Attention is called to the following features of Figure 2.12. (1) The low energy end of the neutron spectrum is emphasized at the expense of the high energy part. (2) The comparitive lack of neutrons at 6 MeV predicted by Hess and measured by Stewart is suggested, but not proven. (3) The rise in neutron flux at 9.6 MeV, found by Stewart but not calculated by Hess, appears to come in at about 9.0 MeV. (4) A disturbing feature are the measurements at 8.2 and 8.6 MeV, when the calculations from the 13 x 13 and 6 x 6 matrices overlap. The 6 x 6 calculation gives a neutron flux lower than that of the 13 x 13 calculation and outside the limits of statistical errors. It appears that a systematic error may have crept in here.

It is conceivable that the overemphasis on the low energy part of the spectrum is due to replacing the unknown values of the cross sections of the upper right hand corner of Figure 2.5 by zero. Only further investigation of the physics of the Si^{28} (n, q) interaction can clear this up. At the same time, it should perhaps be emphasized that the gross features of a fast neutron spectrum can be reproduced relatively easily with this system provided one is satisfied with 400 keV resolution.

REFERENCES

1. H. E. Johns, L. Katz, R. A. Douglas and R. N. H. Haslam, Phys. Rev. 80, 1062 (1950).

2. A. S. Penfold and J. E. Leiss, Phys. Rev. 114 , 1332 (1959).

3. K. N. Geller and E. G. Muirhead, Nuclear Instruments and Methods, 26, 274 (1964).

4. G. Andersson-Lindström - Thesis, University of Hamburg (1964),
    Unpublished. G. Andersson-Lindström and E. Rössle, Physics
    Letters 5, 71 (1963). Cf. Reference 6.

5. B. Mainsbridge, T. W. Bonner and T. A. Rabson, Nuclear Physics
    48, 83 (1963).

6. J. R. Stehn, M. D. Goldberg, B. A. Magurno and R. Wiener-Chasman,
    Neutron Cross Sections I, BNL-325, Brookhaven National Laboratory
    (1964).

7. D. J. Hughes, Encyclopedia of Physics XLIV, 390, Springer, Berlin
    (1959).

8. L. Cranberg, G. Frye, N. Nereson and L. Rosen, Phys. Rev. 103,
    662 (1956).

9. The RAND Corporation, A Million Random Digits with 100,000 Normal
    Deviates, Free Press, Glencoe, Illinois (1955).

10. L. Stewart, Phys. Rev. 98, 740 (1955).

11. W. N. Hess, Ann. Phys. 2, 115 (1959).
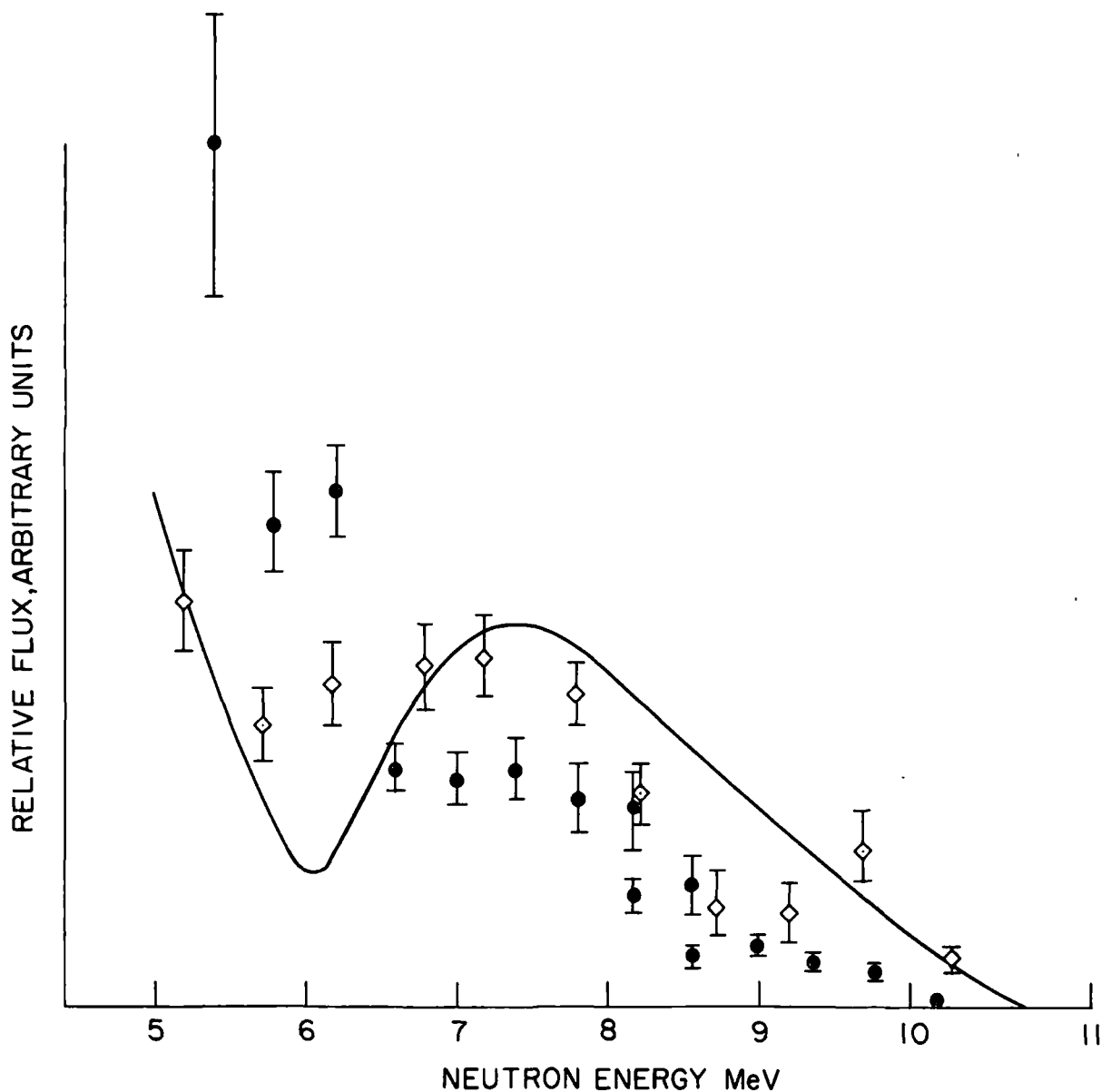
12. A. C. G. Mitchell, Revs. Mod. Phys. 22, 36 (1950).

Figure 2.12.   Pu-α-Be Spectrum as measured with present system compared
with a photographic emulsion measurement and a calculation
which assumes the residual nuclei in the Be (α, n) C reaction
are left in their ground state.

● Present Work
◇ Photographic Emulsion Measurement[10]
— Calculation[11]

28

III. MEASUREMENTS

A. GENERAL

The system elements required for studying the reactions Si(n, q) consist of a neutron source, a silicon crystal with a suitable sensitive volume, and appropriate measuring and recording equipment. Figure 3.1 is a sketch of the system which was used in making the measurements included in this report. Deuterons are accelerated in an electrostatic accelerator to energies of several MeV, the exact energy depending on the neutron energy required. Some of the neutrons produced by the D (D, n) He^3 or T (D, n) He^4 reaction are intercepted by the silicon crystal. These neutrons may induce the Si (n, p) Al or Si(n, α) Mg reaction and the resultant charged particle pairs will lose energy by ionization and other processes in the silicon.

For charged particles, it appears that the coefficient for electron-hole production in silicon is a constant, independent of the type and momentum of the particle involved. The numerical value of the ionization coefficient is approximately 3.5 eV/ion pair. This means that the total energy of the charged particle pairs is proportional to the total charge deposited in the crystal. By means of a special form of feedback amplifier, one may generate an output signal which is proportional to the ionization charge and independent of other parameters. Using a multichannel analyzer, this output signal is sorted into any of 400 bins according to the charge deposited. The number of counts in each channel is recorded photographically, for convenience, and digitally by a printout system for detailed analysis. A list of the equipment issued in these tests is given in Appendix C.

There are two reasons why neutrons generated by the D (D, n) He^3 and T (D, n) He^4 reactions are particularly suitable for these measurements. First, the neutron production cross sections are well known for these reactions.[1] Secondly, there are no excited states of the residual He^3 or He^4 nuclei which means that the neutron flux is strictly monoenergetic in the center of mass system.[2] However, a number of factors can affect the laboratory energy of the neutrons and each must be kept under control if an
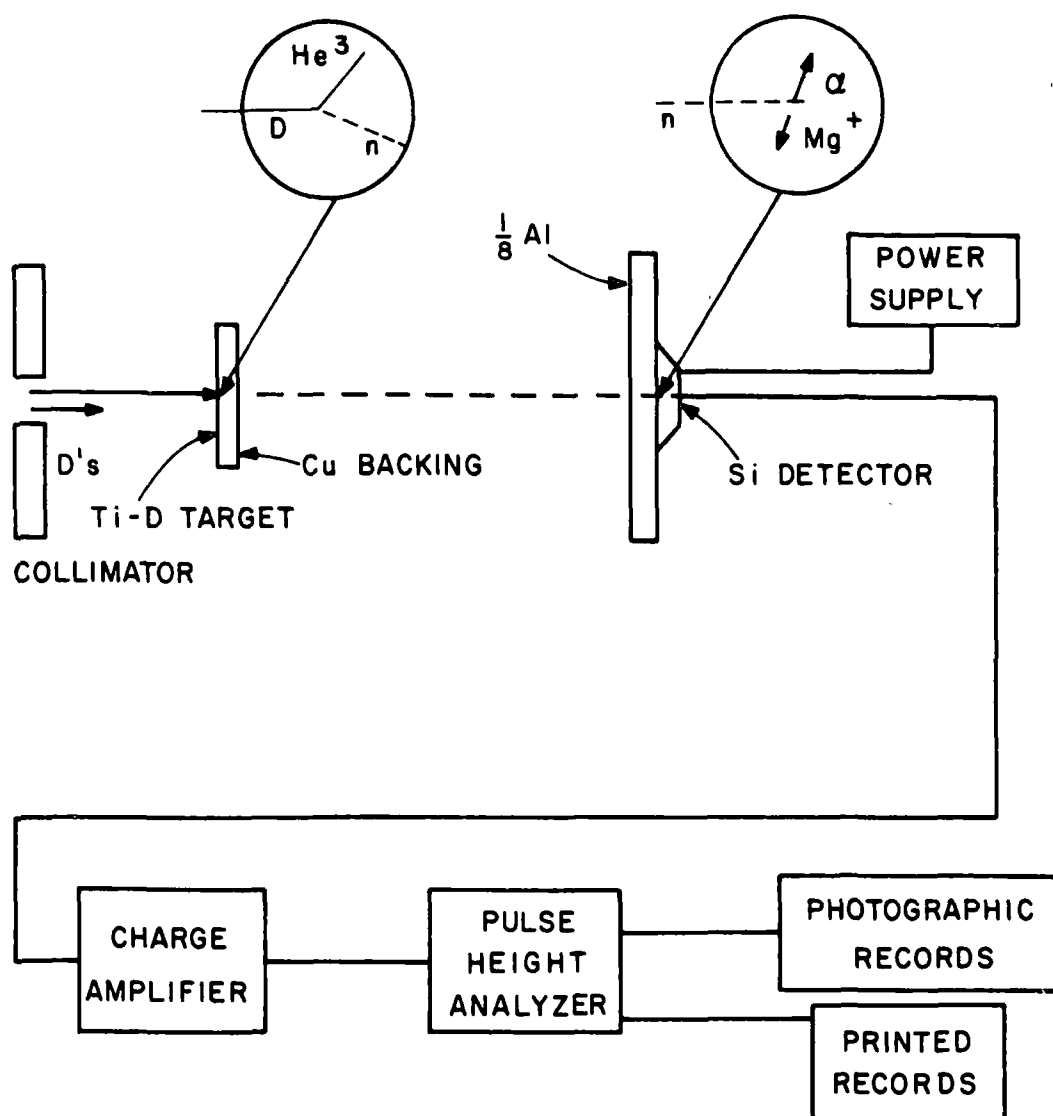
Figure 3.1. Experimental arrangement of equipment used in studying the Si(n, q) reaction.

approximately monoenergetic neutron flux on the silicon crystal is to be obtained. The three most important sources of neutron energy spread[3] are due to (a) the finite thickness of the hydrogenic target; (b) the finite solid angle subtended by the detectors; and (c) thermal agitation in the neutron production target.

In the work reported here, the first two of these factors are more important than the third. They are, in fact, of comparable magnitude and must be considered together to achieve minimum energy spread. Overall neutron energy resolution of 50 keV was considered attainable and the uncertainty due to target thickness, ΔE_{target}, and that due to solid angle considerations, ΔE_{geom}, were adjusted such that

$$(\Delta E_{target})^2 + (\Delta E_{geom})^2 \le (50 \text{ keV})^2 \qquad (3.1)$$

Although the uncertainties encountered in each case are not strictly gaussian, a formula like 3.1 should be sufficiently accurate for practical purposes.

If ΔE_{target} is to be minimized, a thin target is required. The thinnest commerically available deuterated and tritiated titanium targets were obtained. These consist of the hydrogen isotope bonded chemically to a titanium matrix, the whole being deposited on a copper or silver backing 0.010" thick as shown in Figure 3.2. Approximately one hydrogenic atom is bound for each Ti atom.[4]

Deuterated targets with 0.31 mgm/cm^2 of deposited Ti were purchased from the United States Radium Corporation, Morristown, New Jersey. The deuterium density is 1.62×10^{-5} gm/cm^2 (5×10^{18} D's/cm^2). A similar tritiated target was obtained from High Voltage Engineering Coroporation, Burlington, Massachusetts. The Ti is of the same thickness so that there is the same molar concentration of tritium in this target. As absolute cross section measurements were not attempted, the target thicknesses are nominal and are required to stay the same or to be calculable, throughout a run.
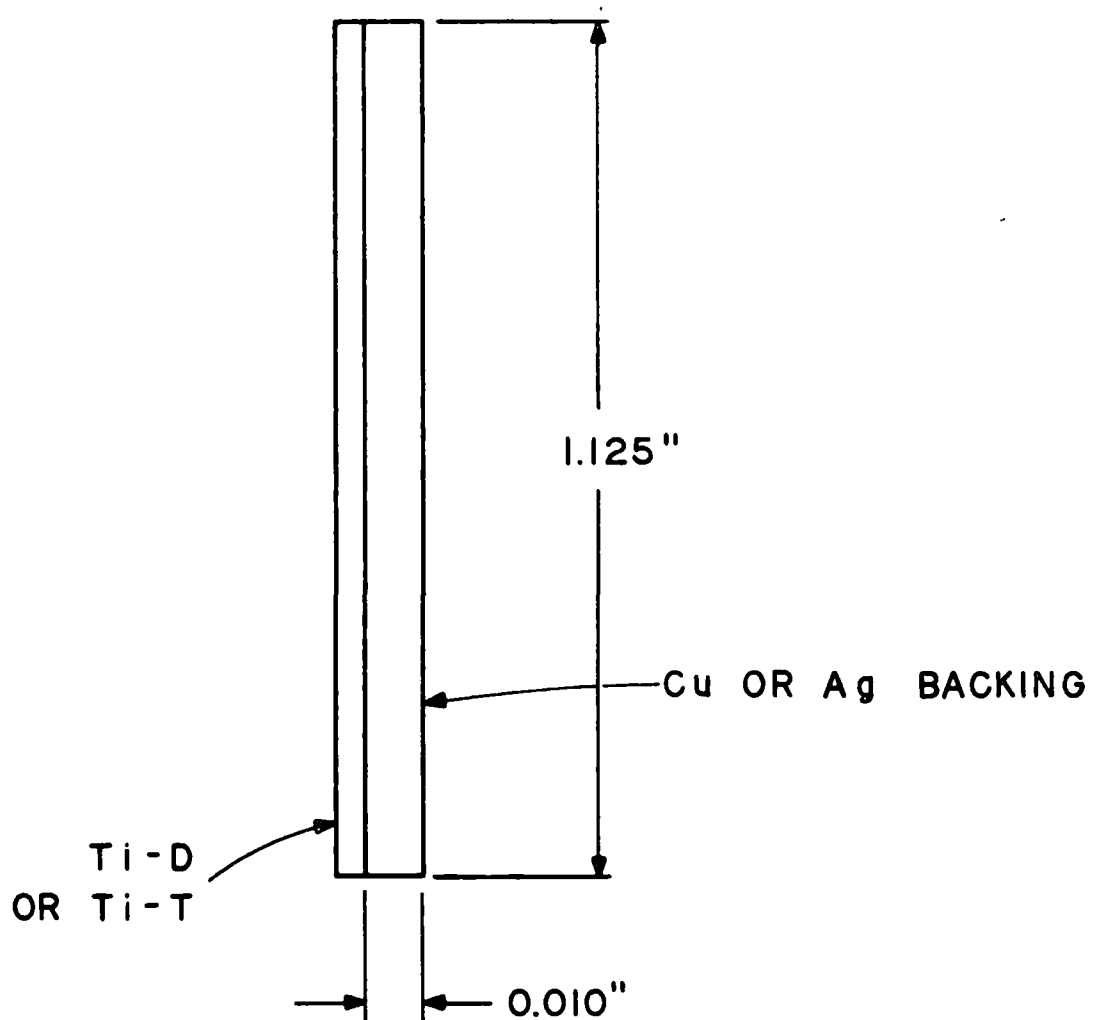
Figure 3.2. Side view of deuterated or tritiated disc. Dimensions are in inches.

The spread in neutron energy due to finite target thickness is due mainly to the ionization loss of the deuteron beam in the Ti matrix. The energy loss of a deuteron beam due to such ionization may be taken from data presented by Whaling[5], and the corresponding spread in neutron energy may then be calculated, giving ΔE_{target}. The energy spread due to the finite sizes of the deuteron beam and of the silicon detector, ΔE_{geom}, were then approximated as follows. For a given neutron energy, the allowed geometry uncertainty is taken from equation 3.1. Tables of reaction kinematics[6] give the allowed angle subtended by the target detector system, θ of Figure 3.3. The allowed distance of the detector from the production target then follows from

$$L = \frac{d_{beam} + d_{det}}{2 \cdot \theta} \tag{3.2}$$

where d_{beam} and d_{det} are the diameters of the beam and detector shown in Figure 3.3. The largest distance of production target to crystal target calculated from equation 3.2 was used throughout a particular run. The overall collection efficiency is affected by only a small factor and such an arrangement is much more convenient than changing this distance every few runs.

B. CRYSTAL DETECTORS

The silicon detectors used in these measurements are of the gallium diffused p-n junction type. The surface is contoured so that surface breakdown at the p-n junction, the usual mode of failure in such a crystal, is inhibited. Since contoured crystals can be biased to considerably higher fields than other types of silicon detectors, one may expect a greater degree of radiation resistance than one finds in a surface barrier type of detector, for example.

Detectors designated 1-11-139 and 1-11-140 were fabricated during the month of January for these tests. The base resistivity of the n-region was about 700 ohm-cm. These crystals were originally procured from Merck with a resistivity of 1750-2000 ohm-cm. Gallium was diffused to a depth of about 50μ at 1250°C. An unwanted but unavoidable result of the diffusion process is the simultaneous lowering of base resistivity, in this case to the aforementioned 700 ohm-cm.
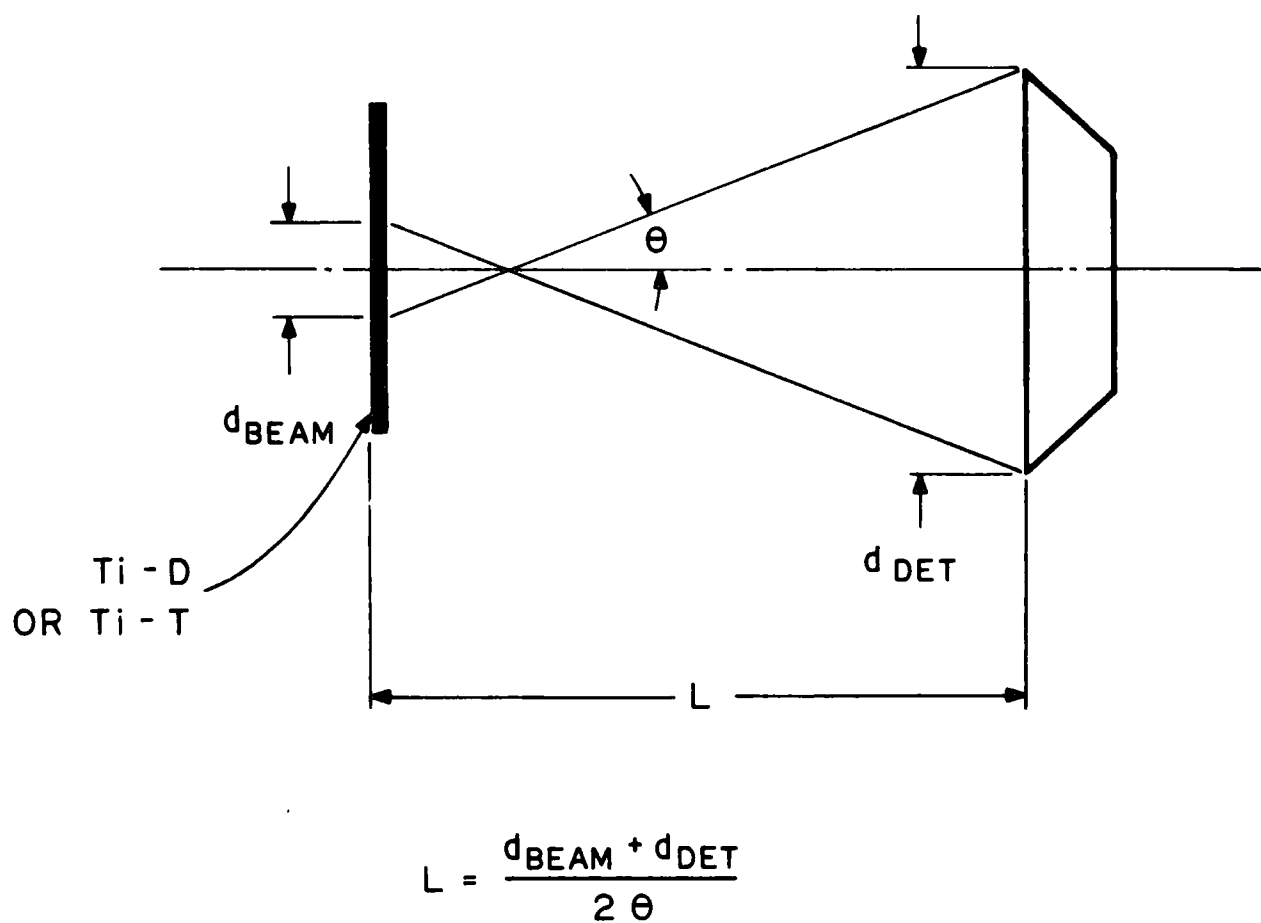
33

$$L = \frac{d_{BEAM} + d_{DET}}{2\,\theta}$$

Figure 3.3.   Diagram illustrating geometry of the deuteron beam, the
detector and the angle θ subtended by the detector.

After diffusion, about 50 μ is lapped from one side, the result being a pillbox with an n-p junction 51 μ from the unlapped side. Subsequent grinding, polishing and etching result in the final contour shown in Figure 3.4.

Further details of the processing of a contoured diode are contained in a previous report.[7]

The sensitive volume of the crystal sketched in Figure 3.4 bears a simple relation to the bias. The width of the sensitive region is given by

$$W = 16.3\sqrt{V} \qquad (3.3)$$

In the above formula, W is in micron if the bias, V is taken as Volts.

The bias must be a compromise between noise and depletion depth, both of which increase with bias. A bias setting of 500 Volt, corresponding to 360 μ depletion width was used throughout these measurements. The noise figure at this setting was about 17 keV FWHM.

C. LOW ENERGY MEASUREMENTS

During the period 27 January - 1 February, a number of exposures were made using the facilities of the Duke University 3 MeV Accelerator. We wish to acknowledge the cooperation of E. G. Bilpuch and his staff in making these exposures. As noted below, Dr. Bilpuch was able to operate the machine at 3.5 MeV, considerably above its rating.

Figure 3.5 shows some of the details of target mounting during these runs. Notice that forced air cooling was used and that as a result a relatively simple mounting system sufficed. Beam currents of 4.2 - 4.5 μa were available and were used.

The runs may be divided into two series, a low energy series where the D(D, n) He^3 reaction was used for neutron production and a high energy series employing the tritiated target disc and the T (D, n) He^4 reaction.

For the low energy runs, the target detector distance, L in Figure 3.3, was held constant at 3.11 cm. This eliminated a further variable to be taken into account in reducing the data and at the expense of lowering counting efficiency by 10% or less.
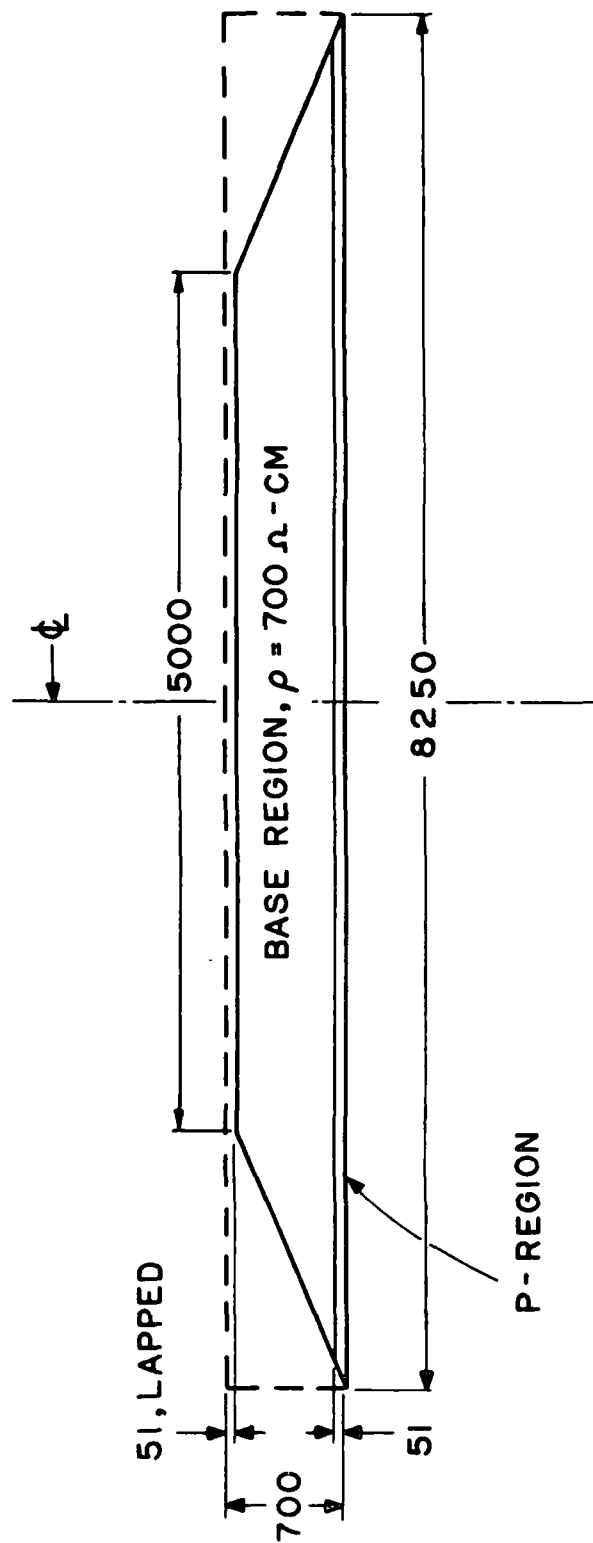
Figure 3.4. Dimensions of crystal detectors 1-11-139 and 1-11-140. Length in microns (.001" = 25.4 μ). Dashed lines show outline of original pillbox from which the contoured detector was ground.
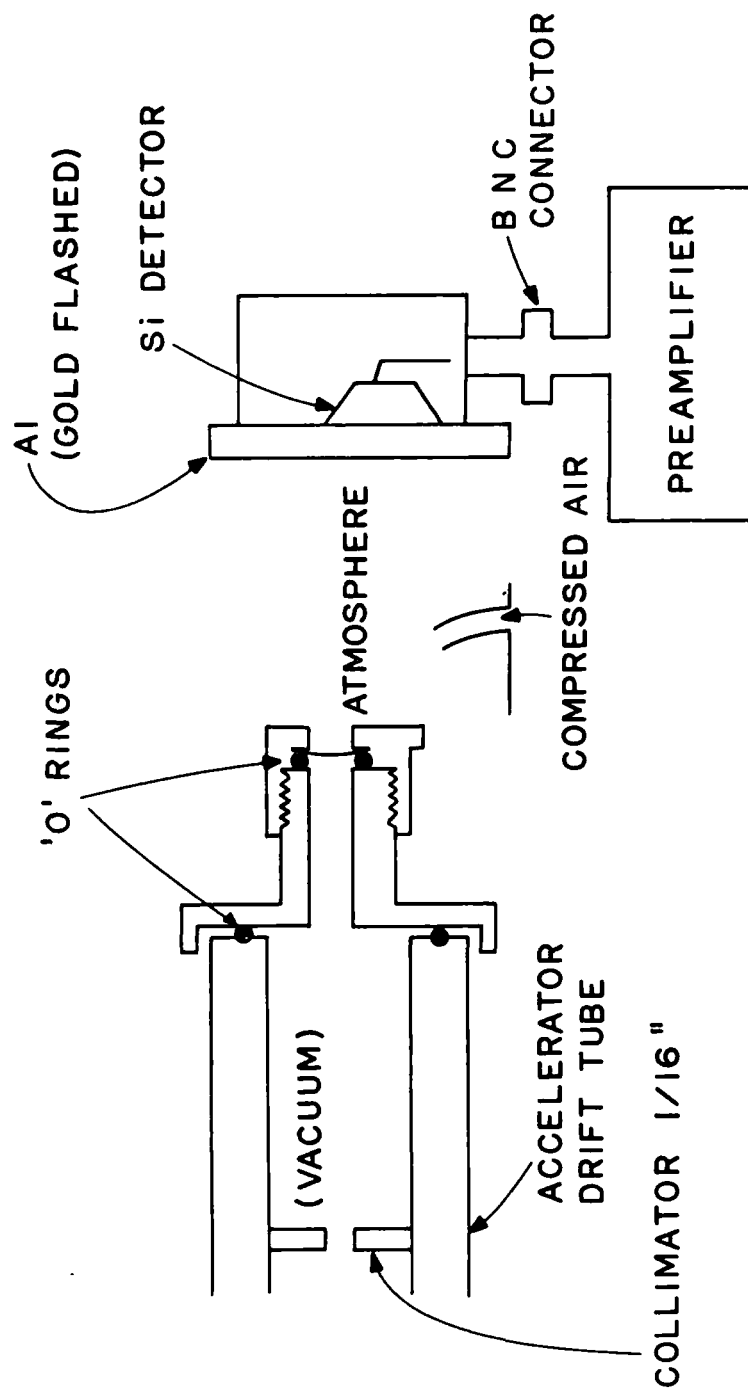
Figure 3.5. Target details at Duke University exposures.

A total of 30 runs were taken using the D (D, n) He^3 reaction. Deuteron energy was varied in 50 keV steps from 1.682 MeV to 3.5 MeV. This corresponds to neutron energies between 4.9 MeV and 6.8 MeV.

Figure 3.6 shows the results at 5.95 MeV and 6.00 MeV using 2000 μc of integrated deutron current. Only the n, α_0 and n, p_0 + p_1 disintegrations are resolved. Some indication of the Si^{29} (n, α_0) and Si^{29} (n, α_1) disintegrations are present although the statistics are very poor.

Figure 3.7 shows the results around 6.3 MeV neutron energy. A Si^{28} (n, α_1) resonance is present and the Si^{29} (n, α) interaction is more pronounced.

Besides the runs recorded in Figures 3.6 and 3.7, records of other runs are available such that the charged particle disintegrations of silicon between 4.9 MeV and 6.8 MeV could be worked out. Indeed, this was the original purpose behind these exposures. As the work of Andersson-Lindström and of the Rice group has come to our attention, and as this would be essentially a reproduction of their work, we have devoted our analysis efforts on the energy region not covered by their work and have assumed their cross sections to be correct.

D. HIGH ENERGY MEASUREMENTS

An investigation of the Si (n, q) reaction in the neutron energy range 8.2 - 10.6 MeV was carried out. Through the courtesy of W. E. Stephens, the facilities of the University of Pennsylvania's Tandem Accelerator were made available to us during the period of 20 - 22 of February. Round the clock operation of the accelerator was performed by the Penn operating staff of C. T. Adams, D. Freil and J. Morgianis. Representing G. E. were R. A. McKinney, J. A. Shannon and J. B. Trice.

The deuterated target used during these exposures was water cooled, as shown in Figure 3.8 About 2.7 μa of deuteron current was available. The distance between the production target and the silicon target was 12.2 cm.

A total of 31 runs was made. Table 3.1 lists for each run the neutron energy and the integrated deuteron current. A typical result was shown as

a.   Neutron Energy of 5. 95 MeV
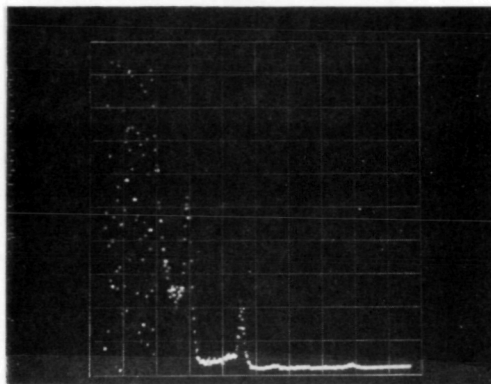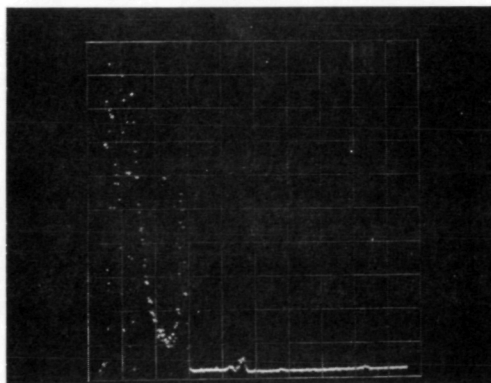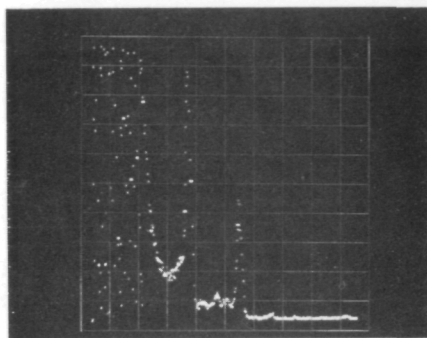

b.   Neutron Energy of 6. 00 MeV
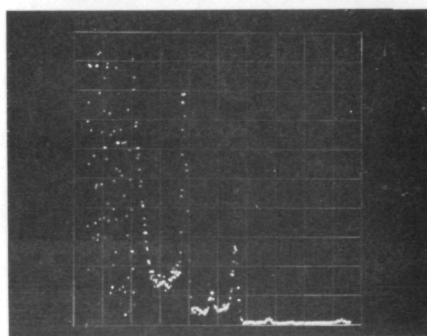

FIGURE 3. 6 - Charged Particle Spectrum at Neutron Energy of 5. 95 MeV
        and 6. 00 MeV.

a.   Neutron Energy - 6. 3 MeV

b.   Neutron Energy - 6. 35 MeV

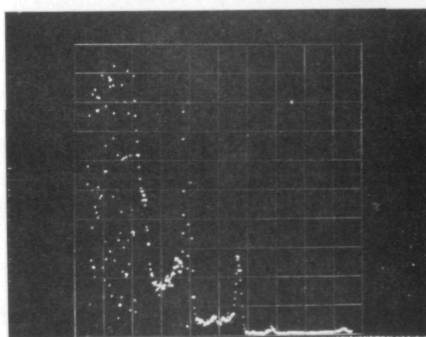c.   Neutron Energy - 6. 40 MeV

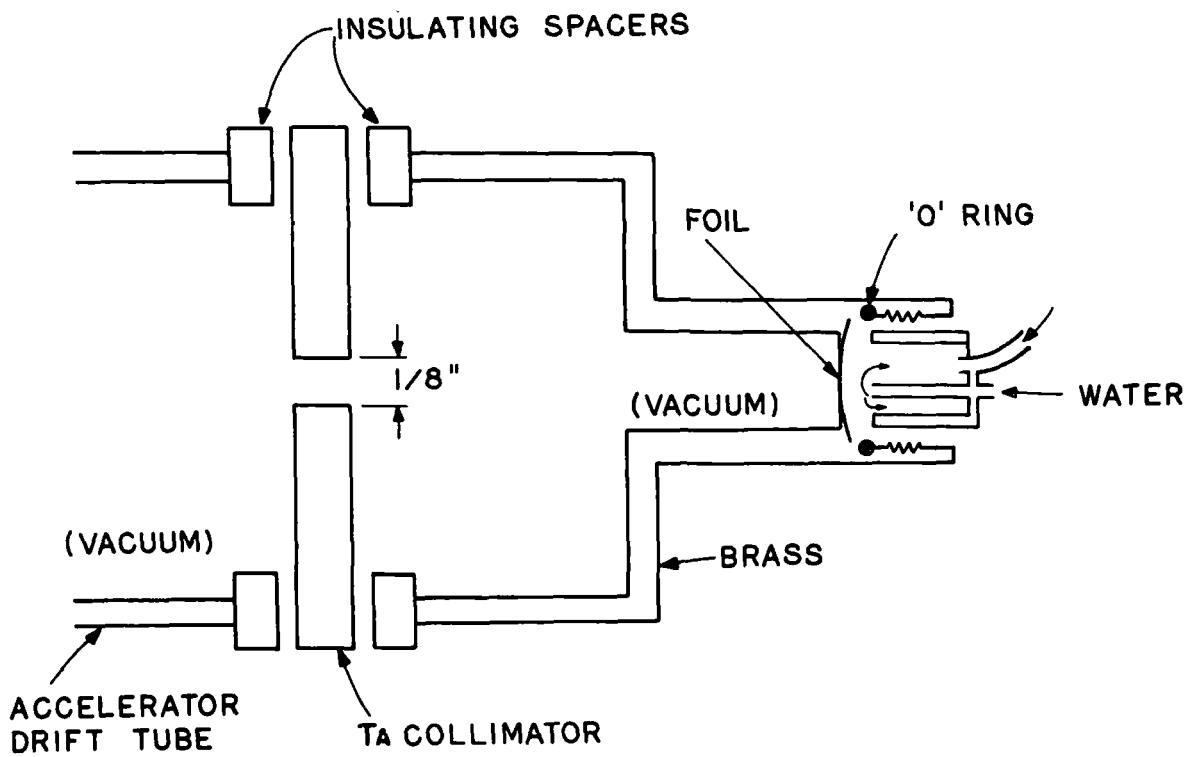FIGURE 3. 7 - Charged Particle Spectrum near 6. 3 MeV Neutron Energy.

40

Figure 3.8.   Details of Water Cooled Target as Used at the Penn Tanden, the Si Target Mount was identical to that used at Duke, (Figure 3.5.).

Figure 2.1 on page 5 . In general, runs with less than 4000 microcoulomb integrated current did not have sufficient statistics to give good results.

The counts under the peaks corresponding to the (n, q) reactions leading to various final states were evaluated. Corrections for finite target thickness was made as in Appendix D. Normalization of σ $(Si^{28} (n, \alpha_0) Mg^{25})$ = 100 mb at neutron energy of 8.2 MeV was assumed.

The most reliable results are shown in Figures 3.9 and 3.10. The flags represent only counting errors computed as

$$\frac{\Delta \sigma}{\sigma} = \frac{\sqrt{\text{Total counts}}}{\text{Total counts - Background}}$$

Figure 3.9 shows the (n, p) results from 9.5 to 10.2 MeV. In addition to the points shown, p_4 and p_5 peaks were observed as follows:

Neutron Energy	p_4	p_5
9.5 MeV	4.8 mb	9.3 mb
9.6 MeV	8.2 mb	8.7 mb
9.7 MeV	16.2 $(p_4 + p_5)$	

The (n, α) cross sections are shown in Figure 3.10. An additional broad peak at the higher neutron energies which may be attributed to the $p_4 + p_5 + \alpha_6 + \alpha_7$ has a value of 66 mb at 9.9 MeV and 160 mb at 10.1 MeV.
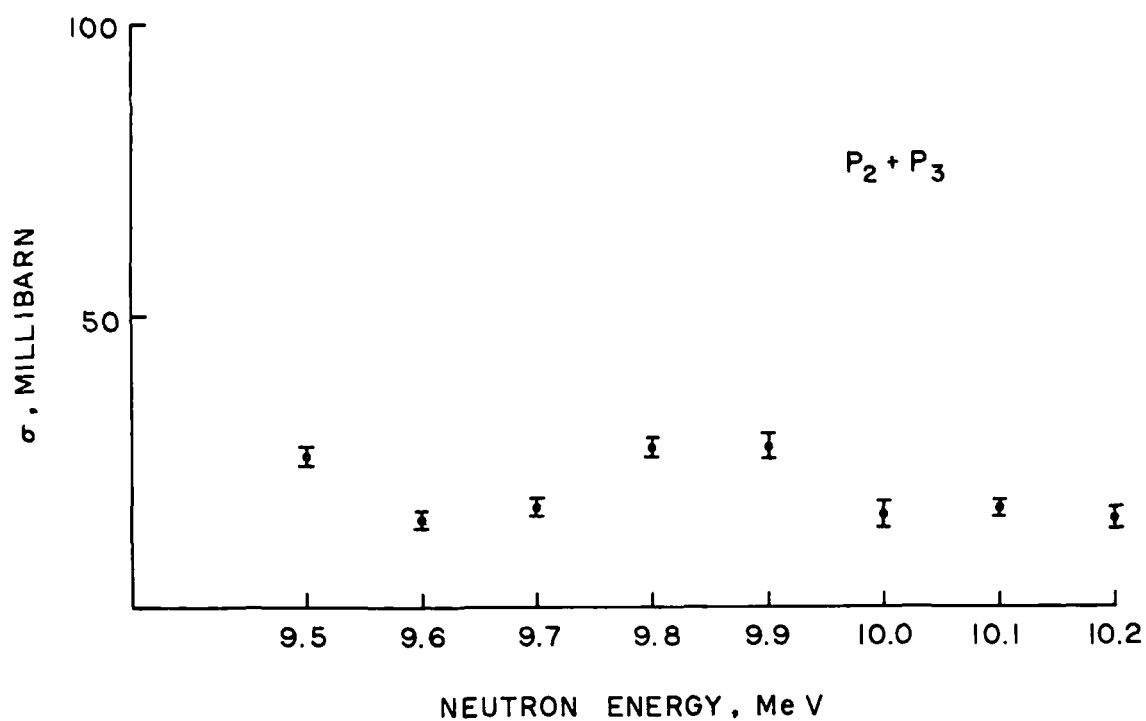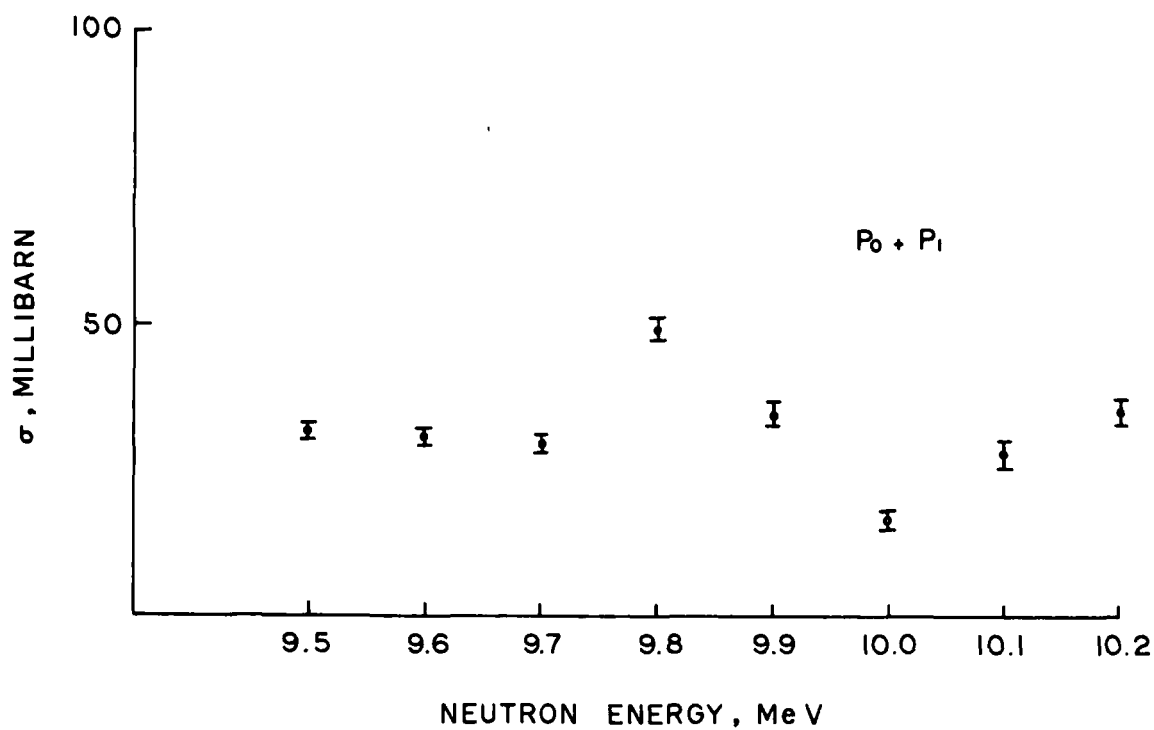
FIGURE 3. 9   Si (n, p) Cross Sections to various final states.   (a) The Si(n, $p_0 + p_1$) Cross Section.   (b) The Si (n, $p_2 + p_3$) Cross Section.   Flags represent counting errors.

σ, MILLIBARN

100

50

9 5   9 6   9 7   9 8   9 9   10 0   10 1   10 2

NEUTRON ENERGY, Me V

α_0

σ, MILLIBARN

100

50

9 5   9 6   9 7   9 8   9 9   10 0   10 1   10 2

NEUTRON ENERGY, Me V

α_1

σ, MILLIBARN

100

50

9 5   9 6   9 7   9 8   9 9   10 0   10 1   10 2

NEUTRON ENERGY, Me V

α_2

Figure 3.10 $Si^{28}(n, \alpha) Mg^{25}$ Cross Sections to various final states. Flags represent counting errors. α_0: Mg^{25} ground state. α_1: Mg^{25} first excited state, etc.
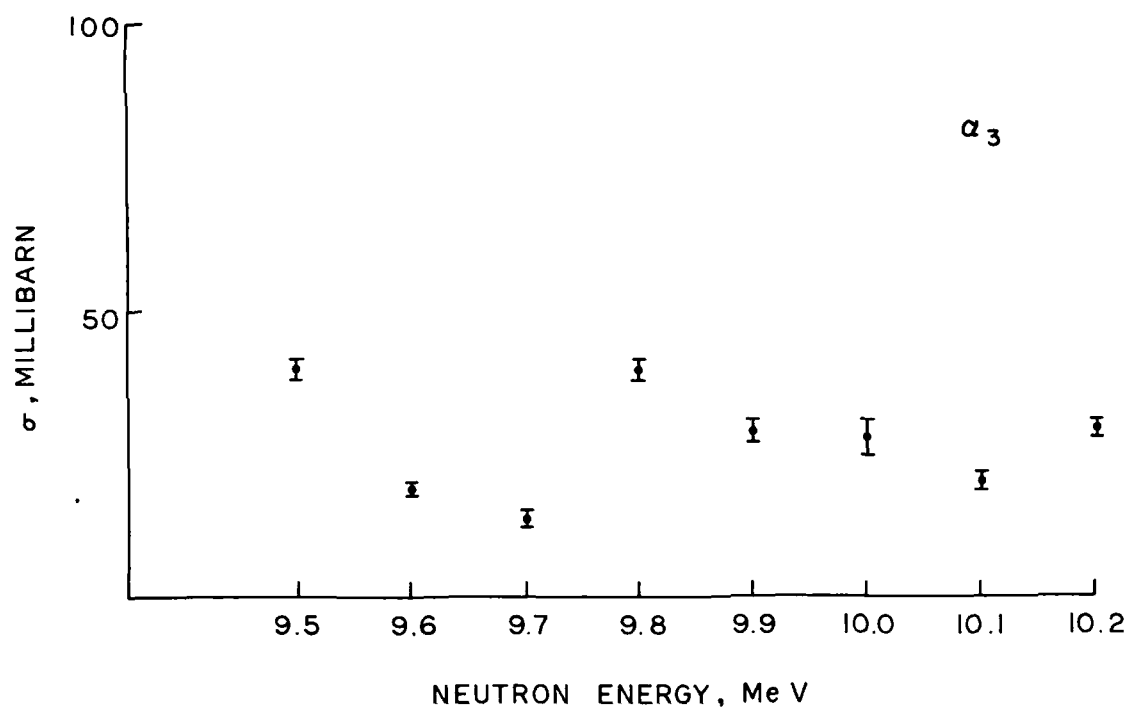
Figure 3.10   (Continued)

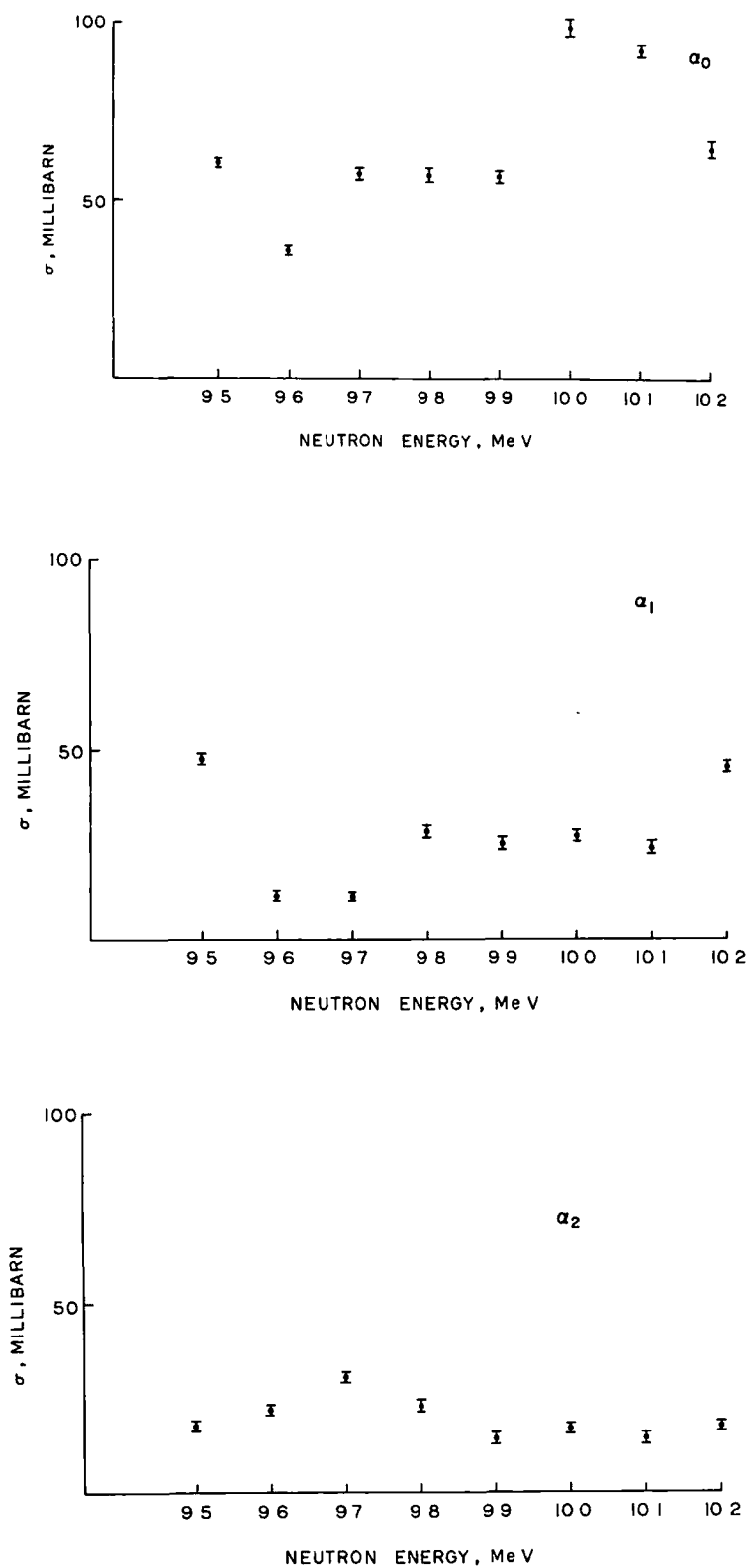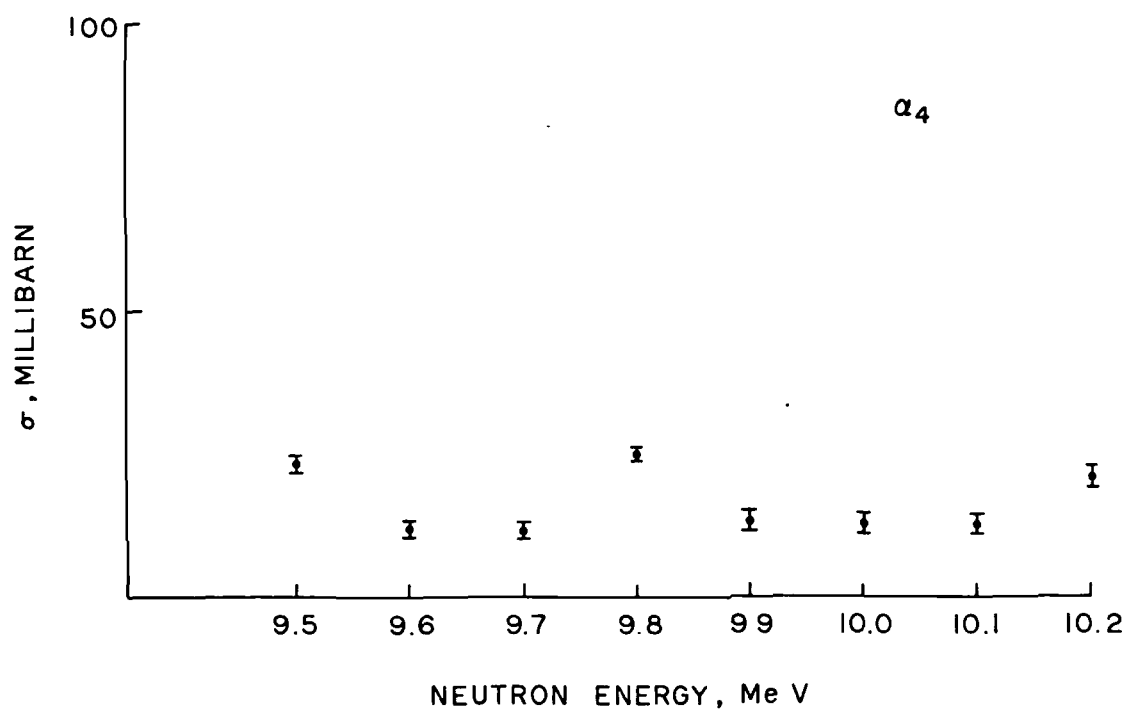# TABLE 3.1

Some details of Neutron Exposures taken at the Penn Tandem, 20 February - 22 February, 1965.

NEUTRON ENERGY	TOTAL CHARGE ON TARGET	DAY OF MONTH
8.2 MeV	3,000 μc	20
8.2	4,800	21
8.2	2,400	22
8.3	4,000	20
8.5	2,000	20
8.6	1,000	20
8.7	1,000	20
8.8	1,000	20
8.9	1,000	20
9.0	4,800	21
9.2	7.988	21
9.3	2,000	20
9.3	7.535	21
9.4	9.448	21
9.5	2,000	20
9.5	19,284	21
9.6	18,987	21
9.7	19,736	21
9.8	15,809	21
9.9	2,000	20
9.9	14,966	21
10.0	14,946	22
10.1	15,574	22
10.2	2,000	20
10.2	17,260	22

TABLE 3.1(continued)

NEUTRON ENERGY	TOTAL CHARGE ON TARGET	DAY OF MONTH
10. 3	2, 000	20
10. 3	4, 800	21
10. 4	4, 800	21
10. 4	31, 341	21
10. 5	4, 800	21
10. 6	4, 800	21

REFERENCES

1. J. E. Brolley, Jr. and J. L. Fowler in Fast Neutron Physics I, Marion and Fowler eds, Interscience, New York (1960).

2. R. L. Henkel, J. E. Perry, Jr. and R. K. Smith, Phys. Rev. 99, 1050 (1955).

3. J. Monahan in Fast Neutron Physics I, Marion and Fowler, eds. Interscience, New York (1960).

4. E. R. Graves, A. A. Rodrigues, M. Goldblatt and D. I. Meyer, Rev. Sci. Inst. 20, 579 (1949).

5. W. Whaling, Encyc. of Physics XXXIV, 193, Springer, Berlin (1958).

6. L. Blumberg and S. I. Schlesinger, AECU-3118, Los Alamos (1956).

7. J. B. Trice, G. C. Huth and J. A. Shannon, Design and Development of Surface Contoured Semiconductor Detectors, NAS-8-5395. Unpublished (1964).

IV. TELEMETRY

A. ASSUMPTIONS

It is the purpose of this chapter to show that telemetry technology is capable of handling the data which are required as inputs as described in Chapter II. That is to say it is possible to build up a telemetry system from components available today or in the near future such that the neutron spectrometer under consideration may be regarded as a flyable instrument.

We assume throughout this discussion that a pulse height analyzer capable of analysis at 10^6 sec^{-1} is available. This appears to be a major extrapolation from the operation of the usual pulse height analyzer which function at about 2×10^4 sec^{-1}. However when one considers that a 20 kc analyzer works with a train of 2 mc pulses from the analog digital converter and that 20 mc pulse trains and even 200 mc pulse trains should soon be available, the assumption of 10^6 counting rates seems probable within a few years.

Take an overall flux of 10^{12} sec^{-1} cm^{-2} and a detector with area 0.25 cm^2 of thickness 400μ. Counter efficiency for this case is about 10^{-4}. Since about 1% of a typical spectrum falls in the energy range above 5 MeV the total output rate from such a detector is about 10^6 sec^{-1}. This matches the rate to our hypothetical pulse height analyzer.

As counting errors are proportional to the square root of the number of counts, we may prepare a table showing the total counts per channel necessary to give adequate statistics. We call the system with 5×10^5 counts in each channel excellent and the system with 5×10^3 counts good. A system with only 50 or so counts per channel would be inadequate.

Assuming the neutron energy range 5 - 12 MeV is of interest, the charged particle range of 1.5 - 9.4 MeV must be covered. This defines the dynamic range of the amplifier and pulse height analyzer.

We further assume that a channel width of 125 keV is excellent and a width of 560 keV is acceptable. Channel width of 400 keV was used in Chapter II. Thus 64 channels is considered an excellent number 14 and should be acceptable.

TABLE 4.1

Total counts per channel needed to give adequate statistics.

Counts	
5×10^5	There is no point in having more counts than this in any channel
5×10^3	This should be adequate for good statistics
10	Not acceptable

B. SYSTEM

The overall telemetry system is shown as Figure 4.1. Total scalar capacity is 32×10^6 for the excellent system and 7×10^4 for the acceptable system. One requires a string of 19 flip-flops for each scalar (excellent) or 13 for each scalar (acceptable).

The sample time for the excellent system is 35 sec for the good system 0.7 sec. This time is exclusive of transmission time.

Figure 4.2 shows a data compression scheme, allowing a compression of 1.75:1. Assuming 19 flip flops per scalar, four analog words are required to read out a scalar. The first two words describe the flip flop in which the most significant bit is found. The next two words describe the orders of the six most significant bits. This is very similar to writing 3.12×10^5 as .3125. It has an overall maximum error of $2^{-7} = .0078$.

As each scalar requires four analog channels the total channel requirement is 256 channels for the excellent system and 56 for the acceptable system. These numbers are exclusive of certain housekeeping data which must also be monitored.

Allowing 43 channels for housekeeping, one may operate with telemetry band E at a commutation rate of $900 \ \text{sec}^{-1}$. Thus one would have spectral information coming in at $3 \ \text{sec}^{-1}$ (excellent) or $9 \ \text{sec}^{-1}$ (acceptable). One might wish to time share this band with other channels if the time scale in which one is interested is longer than 1/3 sec.

C. POWER AND SPACE REQUIREMENTS

Each channel requires three high speed (~ 1 mc) flip flops and either 16 or 9 slower speed (125 kc) flip flops depending on whether one builds the excellent or the good system. The high speed flip-flops, such as Signetics SE124GDTL require 49 milliwatts of power per channel. Low speed flip flops such as the Company's 4JP365 take one mw per stage. Including the digital/analog converter, each channel takes 90 mw for the excellent system. Total power requirement, exclusive of the pulse height analyzer is thus 6.3 watts.
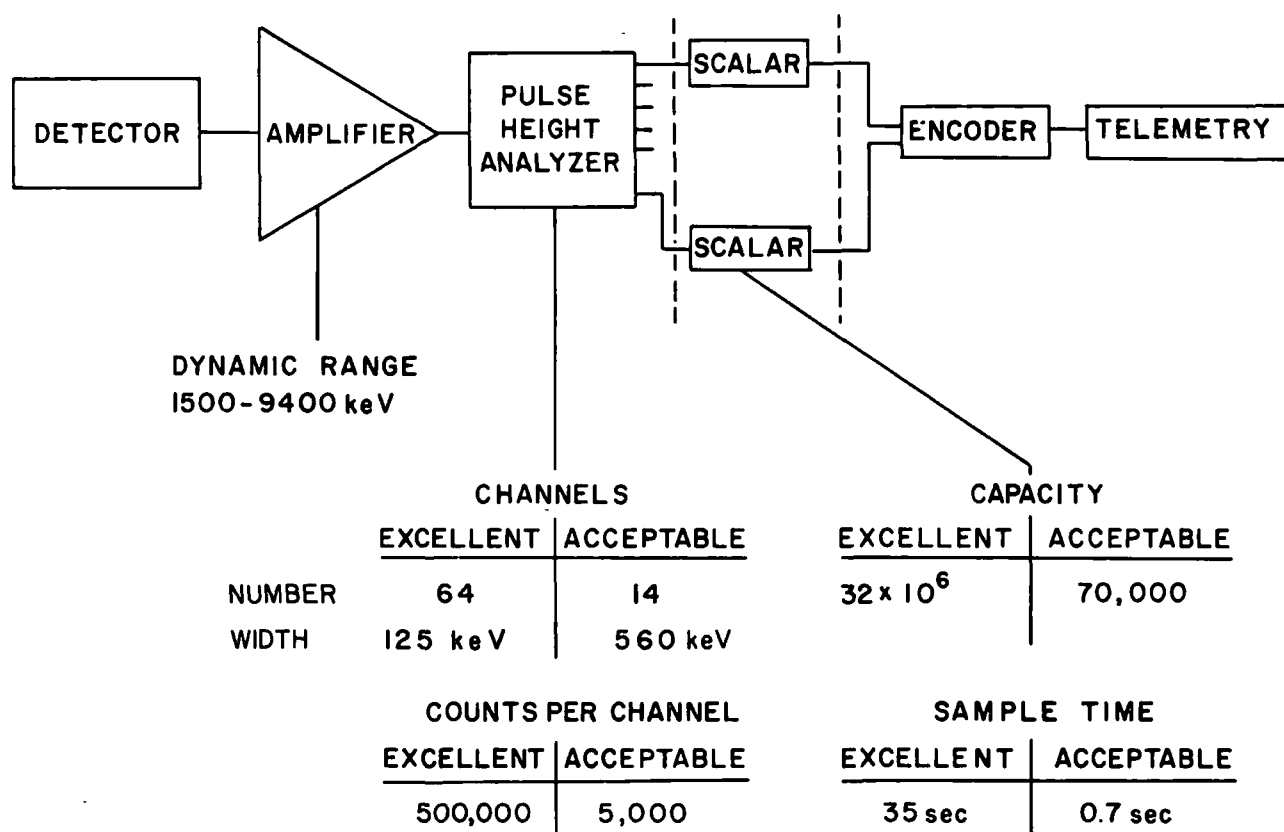
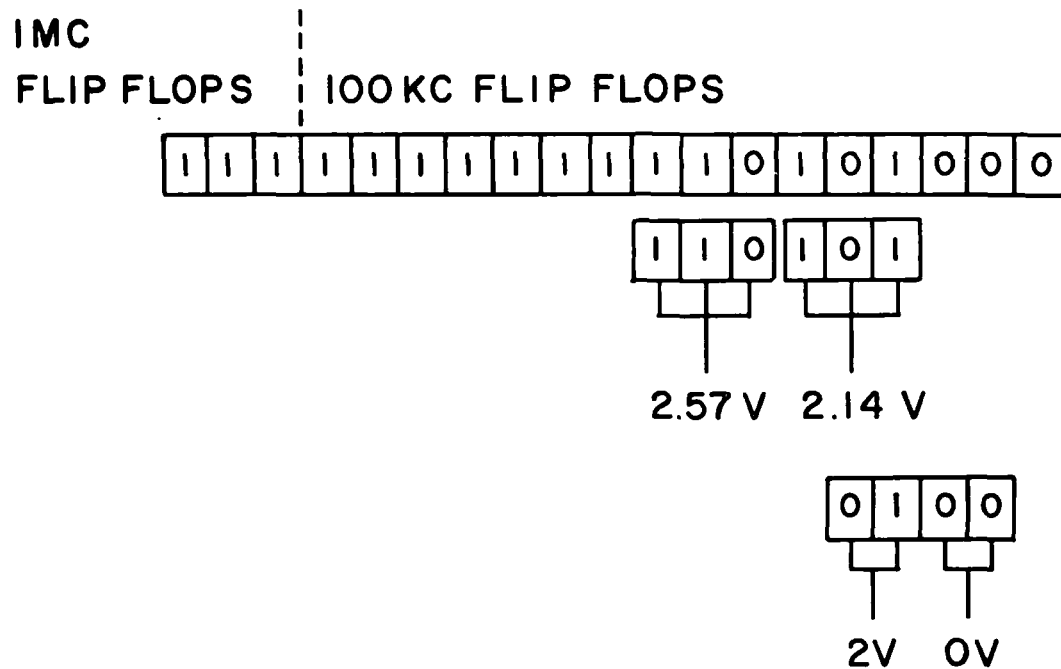Figure 4.1   Overall Telemetry System

Figure 4.2   Data Compression

Packing density of this system can be rather high. It is convenient to speak of this factor in terms of "bugs", one buy being either a flip-flop or an interconnecting network. The name derives from the physical appearance of the devices. Bug density of 33 per cubic inch is possible.

A channel for the excellent system, including D/A conversion requires 58 bugs, that for the good system requires 44 bugs. The volume of the excellent system is then 123 in^3, that of the adequate system 19 in^3.

Thus far we have looked on the pulse height analyzer as a black box to be fitted into the telemetry system. If power and space are at a premium the flip-flops may serve as the memory portion of the pulse height analyzer. Thus one would be designing an integrated analysis - telemetry system.

REFERENCE

1.   M. H. Nichols and L. L. Rauch, Radio Telemetry, Wiley, New York (1960).

V. CONCLUSIONS AND RECOMMENDATIONS

A. NEUTRON PHYSICS

One result of this study is the determination of the various Si^{28} (n, q) cross sections as shown in Figures 3.9 and 3.10. When these measurements are combined with similar measurements in the energy range 5-9 MeV it appears that the various cross sections, integrated over angle, are available below neutron energies of 10.4 MeV.

As practical neutron sources may have high energy limits above 20 MeV, it is recommended that a further extension of the cross section measurements be made. To successfully perform such an experiment a neutron source more sophisticated than the Ti-D target discussed in Chapter III is required. Figure 5.1 shows a system based on a gaseous form of neutron target. With such a target the charged particle background forming the base of the peaks in Figure 2.1 should be virtually eliminated.

The energy interval recommended for studying the interactions is 10-14 MeV in 50 or 100 keV steps. Above 14 MeV energy some measurements using the "14 MeV" neutrons from the T (D, n) He reaction are available.

It appears that the ABACUS-2 program of Elliot H. Auerbach* and others can be programmed to calculate the average values of the various Si(n, q) interactions. The optical model of the nucleus is used. There are fluctuations about these average values which are not susceptible to calculation. This program should be procured and detailed comparison with the experimental data should be made.

B. NEUTRON SPECTROSCOPY

As shown in Figure 2.12 on page 28 it is possible to use the technique discussed in Chapter II to compute out a fast neutron spectrum. The low energy counts in the charged particle spectrum had to be subtracted out before the calculation could proceed. If our analysis of these counts as being due to the β^- decay of Al^{28} is correct, such subtraction will be negligible if time scales of less than two minutes are practicable. In general, this will be
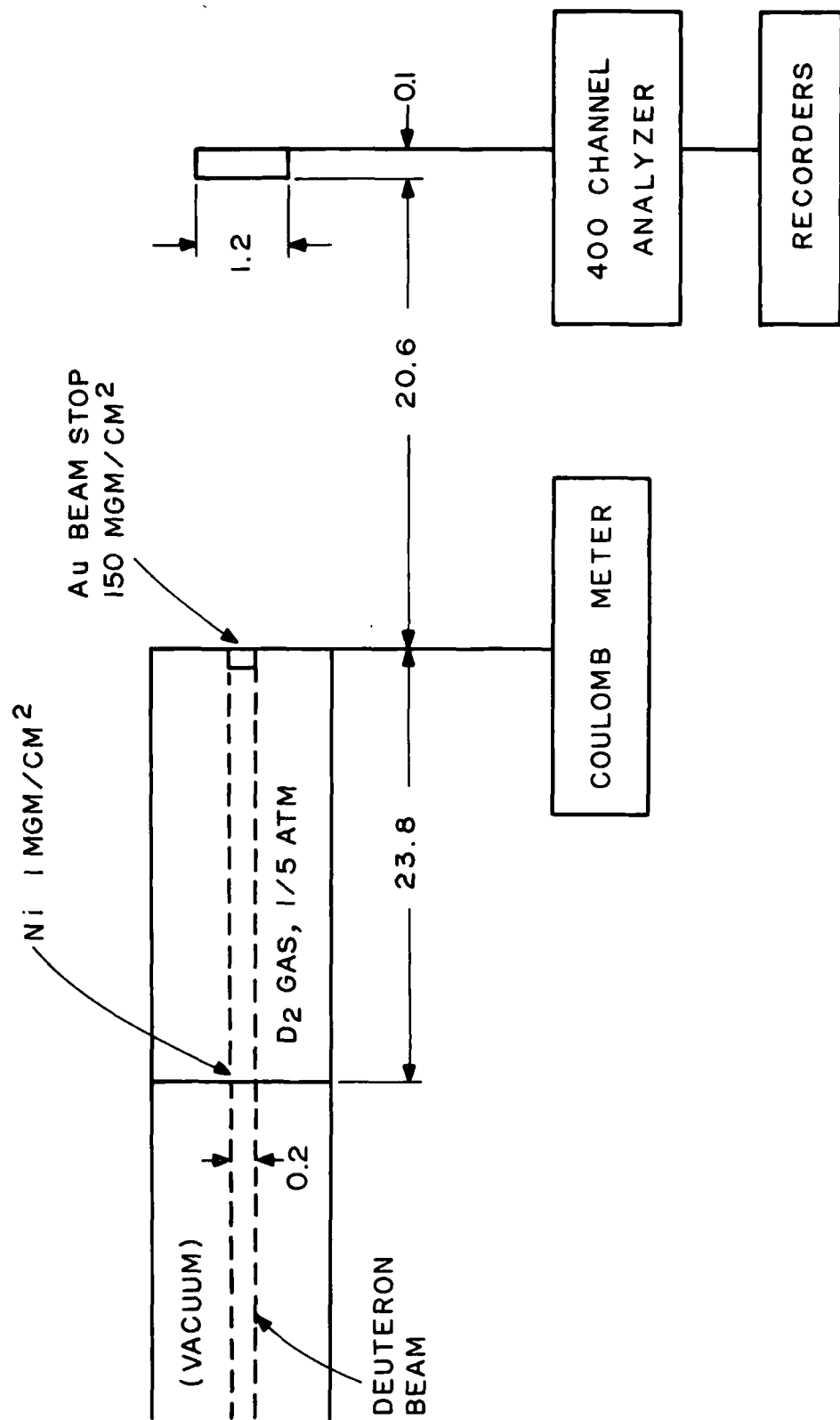
---

*Letter, 1 June 1965.

Figure 5.1. Geometry of a system for measuring Si(n, q) cross sections which uses a gas target for neutron production. Dimensions in cm.

the case for intense sources, i.e., those with neutron flux of the order of $10^6 \text{ cm}^{-2} \text{ sec}^{-1}$. If 10^5 or so counts can be recorded in 10 seconds then the subtraction problem should disappear.

A further source of background is γ-radiation and since the photo cross section of Si is about 1400 mb as opposed to $\sim$200 mb for the Si (n, q) reaction it will be necessary to provide some shielding if the γ-flux is as much as 10% of the fast neutron flux. If this is the case then one will be measuring a somewhat moderated neutron spectrum.

The bin width of 400 keV used as an example in Chapter II is suggested as being adequate. However, if sufficient information processing equipment is available one may in some cases improve this resolution. It is a question of balancing energy accuracy with counting accuracy. If many counts are available energy resolution of 120 keV may be attainable and indeed one of the telemetry examples in Chapter IV is based on such a bin width.

Thicker sensitive regions than those considered above (360μ) are of course desirable, but perhaps not critical. It should be noted that the effective broadening of the (n, p) and (n, α) peaks (Fig. 2.9) amounts to some tens of keV. If high resolution spectroscopy ($\Delta E_n < 50$ keV) is not required then it appears the crystal used in this study should be adequate.

The difficulties of more conventional semiconductors with respect to stability and radiation damage are too well known to be considered here. The surface contoured type used in these studies must be expected to be more resistant to radiation damage than other types of detectors. Their noise figures and stability properties were quite adequate during the course of these investigation.

Should a large number of investigation of spectra be made by this technique, it will be found that calculations on a desk computer rapidly become overwhelming. Although one may then turn to the larger general purpose computing machines, it would perhaps be wise to consider a smaller machine still capable of automatic operation. A generation of such computers appears to be coming of age.

57

It has been suggested that the Si(n, q) interaction may be most useful in neutron spectroscopy if a semiconductor detector could be fabricated out of Si^{29} or Si^{30} [1, 2]. The Q-value of the Si^{29} (n, α_0) reaction is -36 keV so that the effective threshold energy for neutron spectrocopy should be considerably less than the 5 MeV figure quoted above for Si^{28} detectors. A further advantage of detection based on the Si^{29} or Si^{30} isotope is that the cross sections Si^{29} (n, α_0) and Si^{30} (n, α_0) have a large energy range where competition from other reactions, such as Si^{29} (n, α_1) is negligible. Thus the elaborate machinery of Chapter II required to unscramble a spectrum from Si^{28} may be dispensed with.

The obvious drawback to designing a spectrometer based on a Si^{29} or Si^{30} crystal is the difficulty of obtaining gram quantities of the separated isotope. No doubt as the technical community becomes more proficient in handling silicon a detector based on the separated isotope will be constructed. Such a detector, or set of detectors, should prove most useful in neutron spectroscopy, particularly when instrumental size and weight are important.

REFERENCES

1.   M. Birk, G. Goldring and P. Hillman, Nucl. Instruments and Methods **21**, 197 (1963).

2.   B. Mainsbridge, T. W. Bonner and T. A. Rabson, Nuclear Physics **48**, 83 (1963).

ACKNOWLEDGEMENTS

APPENDIX A

Energy Levels and Spins of the Residual Nuclei

Si^{28} (n, α) Mg^{25}

Level	Spin	Energy
α_0	5/2	
α_1	1/2	586 keV
α_2	3/2	974
α_3	7/2	1608
α_4	5/2	1962
α_5	1/2	2566
α_6	(7/2)	2740
α_7	(3/2)	2805
α_8	3/2	3403
α_9	9/2	3412
α_{10}	(5/2)	3909

Si^{28} (n, p) Al^{28}

Level	Spin	Energy
p_0	3	---
p_1	3	31 keV
p_2	(0)	973
p_3	(3)	1017
p_4	1	1372
p_5	(4)	1633
p_6	(2)	2143
p_7	(4)	2207
p_8	(2)	2279
p_9		2490
p_{10}		2589
p_{11}		2663
p_{12}		2988
p_{13}		3011
p_{14}		3102
p_{15}		3294
p_{16}		3347

60

Si^{29} (n, α) Mg^{26}

Level	Spin	Energy
α_0	0	
α_1	2	1803 keV
α_2	2	2941
α_3	(2, 3)	3584
α_4	2	3943
α_5		4319
α_6		4331
α_7		4350
α_8		4830
α_9		4896
α_{10}		4970
α_{11}		5287
α_{12}		5472
α_{13}		5486
α_{14}		5710
α_{15}		6120
α_{16}		6253

Si^{30} (n, α) Mg^{27}

Level	Spin	Energy
α_0	1/2	
α_1	(3/2, 5/2)	990 keV
α_2	1/2	3500
α_3		6750

61

REFERENCES

1. P. M. Endt and C. M. Braams, Revs. Mod. Phys. 29, 683 (1957).

2. R. K. Sheline and R. A. Harlan, Nucl. Phys. 29, 177 (1962).

3. S. Hinds, H. Marchant and R. Middleton, Proc. Phys. Soc. 78 473 (1961).

APPENDIX B

Q-Values and Spins of Levels Expected from the Reactions Si (n, α) Mg and
Si (n, p) Al

Atomic Number of Si Isotope	Type of Reaction and Number of Excited State	Spin	Q-Value X (-1)
29	α_0	0	36 keV
29	α_1	2	1839
28	α_0	5/2	2655
29	α_2	2	2977
28	α_1	1/2	3241
28	α_2	3/2	3629
28	p_0	3	3857
28	p_1	2	3888
30	α_0	1/2	4213
28	α_3	(7/2)	4263
28	α_4	5/2	4617
28	p_2	(0)	4830
28	p_3	(3)	4874
28	α_5		5221
28	p_4	1	5229

Atomic Number of Si Isotope	.Type of Reaction and Number of Excited State	Spin	Q-Value X (-1)
28	α_6		5395 keV
28	α_7		5460
28	p_5	(4)	5490
28	p_6	(2)	6000
28	α_8	3/2	6058
28	p_7	(4)	6064
28	α_9	2	6067
28	p_8		6136
28	p_9		6347
28	p_{10}		6446
28	p_{11}		6520
28	α_{10}		6564
28	p_{12}		6845
28	p_{13}		6868
28	p_{14}		6959
28	p_{15}		7151
28	p_{16}		7204

REFERENCES

1. P. M. Endt and C. M. Braams, Revs. Mod. Phys. $\underline{29}$, 683 (1957).

2. R. K. Sheline and R. A. Harlan, Nucl. Phys. $\underline{29}$, 177 (1962).

3. S. Hinds, H. Marchant and R. Middleton, Proc. Phys. Soc. $\underline{78}$, 473 (1961).

4. F. Everling, L. A. Koenig, J. H. E. Matlauch and A. H. Wapstra, 1960 Nuclear Data Tables $\underline{I}$, National Academy of Sciences, National Research Council, Washington (1961).

APPENDIX C

Commercial Equipment Used in Test Described in Chapter III.

1.   Amplifier, ORTEC Model 201 - 101.

2.   Digital Recorder, Hewlett-Package HO1-562 A.

3.   Power Supply, Power Design Model HV-1544.

4.   Micro-Microammeter, Keithley Model 410.

5.   Pulse Height Analyzer, 400 channel, RIDL Model 34-12.

6.   Oscilloscope Camera, Beattie Model K5.

APPENDIX D

Derivation of Correction Factor for the Wall Effect

Figure D-1 represents the geometry of the silicon detector when properly biased. d_1 represents the thickness of an inactive layer or window on the surface. d_2 is the active region; d_3, a backing of silicon. Charged particles liberated in the active region - d_2 are collected and measured by the external counters.

Suppose n dx charged particles of range R are released in a layer of thickness, dx between x and x + dx. As the neutron attenuation by the crystal is negligible ($\sim 10^{-4}$), n may be taken as a constant. The fraction of these escaping into the dead layer, d_1, is proportional to the solid angle defined by φ in Figure D-1.

$$
\begin{array}{ll}
\dfrac{n}{2} \left(1 - \dfrac{d_2 - x}{R} \right) dx & R > d_2 - x \\[3mm]
0 & R < d_2 - x
\end{array}
\qquad (D\text{-}1)
$$

A number will also escape into the backing region, d_3. Of these latter, a compensating number of charged particles will escape from the backing region into the crystal. The net result will be a degradation in energy definition, but no loss of counts.

From the left hand region, only partial compensation takes place if R > 2d. It is easy to see that if $x < d_2 - d_1$, no "image nucleus" exists to compensate for the lost charge.

Thus the net fraction of charged particles which escape is given by the integral

$$
\frac{1}{2d_2} \int_{\text{lower limit}}^{d_2 - d_1} \left(1 - \frac{d_2 - x}{R} \right) dx \; .
\qquad (D\text{-}2)
$$

The lower limit in the expression depends on whether the range R is greater or less than the depletion depth, d_2

$$
\begin{array}{ll}
\text{lower limit} = d_2 - R & 2d_1 < R < d_2 \\[2mm]
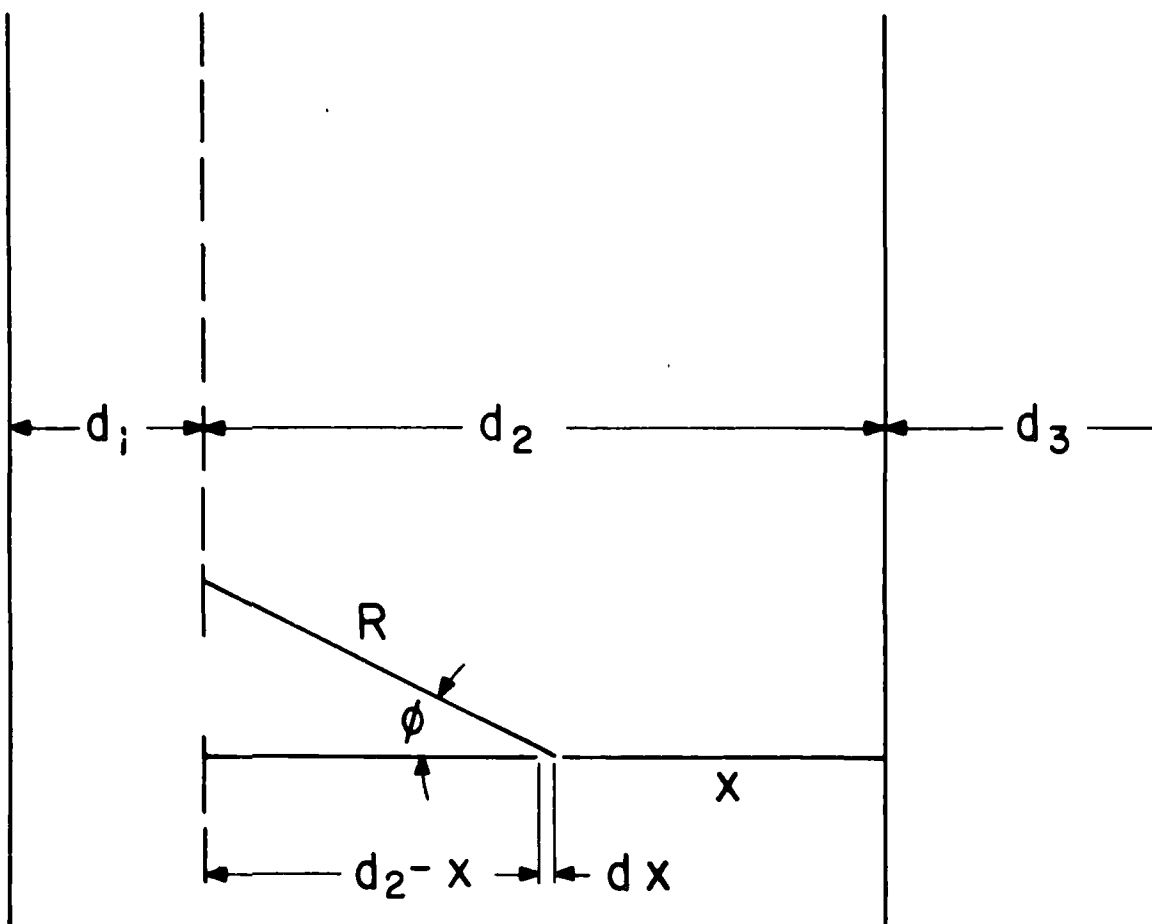\phantom{\text{lower limit}} = 0 & R > d_2
\end{array}
$$

FIGURE D. 1   Geometry of sensitive volume of detector.

d_1 : Inactive Layer

d_2 : Depletion Depth, Active Layer

d_3 : Backing, Inactive

R: Range of Charged Particle

Accordingly, the fraction escaping may be taken as

$$0 \qquad R < 2d_1$$

$$\frac{R}{4d_2} - \frac{d_1}{2d_2} + \frac{d_1^2}{4Rd_2} \qquad 2d_1 < R < d_2 \qquad (D\text{-}3)$$

or

$$\frac{1}{2} - \frac{d_1}{2d_2} + \frac{d_1^2}{4Rd_2} - \frac{d_2}{4R} \qquad R > d_2$$

From the geometry of the silicon crystal, $d_1 = 30\mu$, $d_2 = 380\,\mu$. The fractional loss as a function of proton energy is shown in Figure D-2. The fractional alpha particle loss is zero for all energies encountered in this experiment.
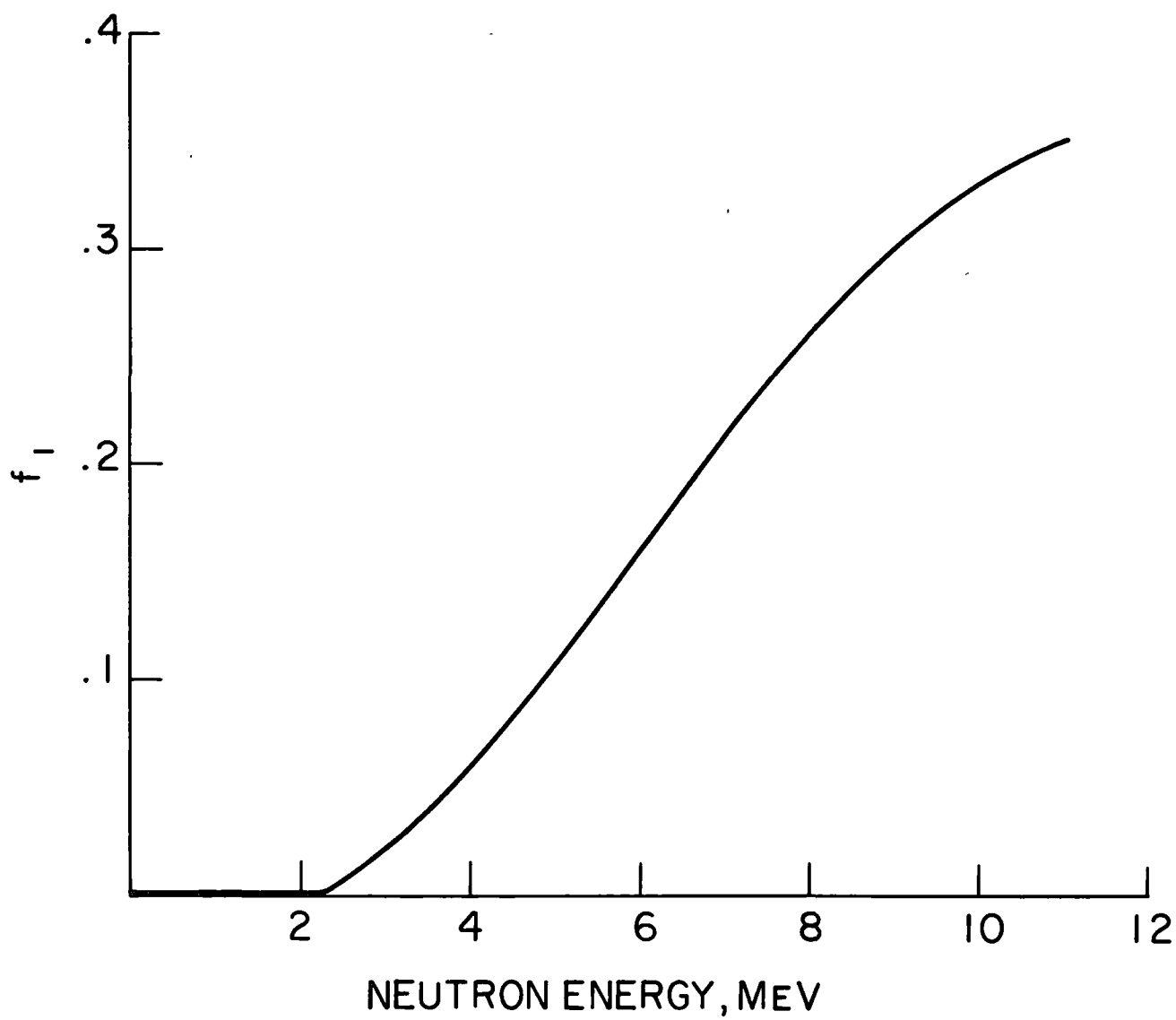
FIGURE D.2. Fractions of protons lost due to wall effect.

Progress Is Our Most Important Product

GENERAL ✸ ELECTRIC